NACA RM A58E19

NACA

# RESEARCH MEMORANDUM

## EXPERIMENTAL INVESTIGATION OF THE EFFECT OF YAW ON RATES OF HEAT TRANSFER TO TRANSVERSE CIRCULAR CYLINDERS IN A 6500-FOOT-PER-SECOND HYPERSONIC AIR STREAM

By Bernard E. Cunningham and Samuel Kraus

Ames Aeronautical Laboratory
Moffett Field, Calif.

NATIONAL ADVISORY COMMITTEE
FOR AERONAUTICS

WASHINGTON
August 26, 1958
Declassified February 8, 1960

NATIONAL ADVISORY COMMITTEE FOR AERONAUTICS

RESEARCH MEMORANDUM

# EXPERIMENTAL INVESTIGATION OF THE EFFECT OF YAW ON RATES OF HEAT TRANSFER TO TRANSVERSE CIRCULAR CYLINDERS IN A 6500-FOOT-PER-SECOND HYPERSONIC AIR STREAM*

By Bernard E. Cunningham and Samuel Kraus

## SUMMARY

A technique has been developed by which air can be shock-compressed by helium to 3660° Rankine to generate a 6500-foot-per-second air stream with a flow duration of 40 milliseconds. The resulting equipment is described. Experiments were conducted to determine rates of heat transfer to transverse circular cylinders of 0.003-, 0.012-, and 0.020-inch-diameter and length-to-diameter ratios greater than 100. The cylinders were tested at a nominal Mach number of 11 with a stagnation Reynolds number (evaluated with free-stream mass flow and stagnation viscosity) of $4.00 \times 10^4$ per foot. For tests normal to the air stream (zero yaw), average Nusselt numbers of these cylinders were found to be in good agreement with earlier data, even though there were large differences in test conditions.

The influence of yaw on rates of heat transfer to the same circular cylinders was investigated at angles of yaw up to 70°. Results of these experiments were compared with earlier data and with theoretically predicted reductions in heat-transfer rates due to yaw. It was found that these heat-transfer rates decreased with increasing yaw angle, $\lambda$, as $\cos^{3/2}\lambda$.

## INTRODUCTION

Intelligent design of hypervelocity vehicles is seriously hampered by the lack of data on the aerodynamic heating which such vehicles will experience in the earth's atmosphere. Some theoretical studies of aerodynamic heating at high Mach numbers have been made for wing leading edges and nose shapes. For example, an approximate theory was developed in

---

*Title, Unclassified.

reference 1 for predicting the rate of heat transfer to a cylindrical stagnation region in hypersonic flight. It was predicted that rates of heat transfer to cylinders at large yaw would be substantially lower than rates of heat transfer to cylinders normal to the air stream, especially in the case where the wall temperature was much lower than the stagnation temperature. It has been theoretically demonstrated by Reshotko and Beckwith (ref. 2) that for compressible laminar boundary-layer flow the effect of yaw on the heat-transfer coefficient at the stagnation line depends markedly on the free-stream Mach number up to values of about 7; thereafter an increase in Mach number does not appreciably influence heat-transfer reductions due to yaw. Goodwin, Creager, and Winkler (ref. 3) have developed correlation parameters, or dimensionless groupings, which can be used to correlate experimental transverse cylinder data and have considered means by which Nusselt numbers can be predicted. In addition, the effect of yaw angle upon local and stagnation point heat-transfer coefficients of transverse cylinders has been treated in reference 3.

The need for heat-transfer data with which the accuracy of these and other theoretical solutions can be evaluated has led to the development of equipment for generating a hypervelocity air stream with flow times up to 40 milliseconds. Heat-transfer data can be obtained in this equipment at higher air-stream-to-body temperature potentials than previously reported (see refs. 1 and 3 through 7, for example). The analysis, construction, and operation of the new equipment are described in this report. An additional purpose of this report is to present heat-transfer data obtained in the new equipment. Average Nusselt numbers of circular cylinders normal to the air stream are presented and compared with other experimental data. Reductions in heat-transfer rates at angles of yaw are presented along with other experimental yaw data and are compared with the predictions of existing theory.

## SYMBOLS

### Primary Symbols

| | |
|---|---|
| $a$ | speed of sound |
| $A$ | cross-sectional area |
| $c_b$ | specific heat per unit mass of body materials |
| $c_p$ | specific heat per unit mass at constant pressure |
| $c_v$ | specific heat per unit mass at constant volume |
| $d$ | diameter |

$\bar{h}$ average heat-transfer coefficient

$k$ coefficient of thermal conductivity

$M$ Mach number

$n$ exponent of temperature in thermal conductivity and viscosity functions, $k \sim T^n$ and $\mu \sim T^n$

$\overline{Nu}$ average Nusselt number based on a length $d_b$ and stagnation temperature conditions, $\frac{\bar{h}d_b}{k_t}$

$p$ static pressure

$p_t$ reservoir pressure

$p'$ pitot pressure

$Pr$ Prandtl number, $\frac{c_p\mu}{k}$

$q$ dynamic pressure

$Q$ average rate of heat transfer per unit area

$R$ gas constant

$r_b$ radius of cylinder

$Re_t$ stagnation Reynolds number, based on cylinder diameter and evaluated with free-stream mass flow and stagnation viscosity conditions

$t$ time

$T$ absolute temperature

$T_t$ absolute stagnation temperature

$u$ stream velocity

$x$ distance along axis of pump tube, measured from diaphragm

$\alpha$ $\frac{\gamma + 1}{\gamma - 1}$

$\beta$ $\frac{\gamma - 1}{2\gamma}$

$\gamma$ $\frac{c_p}{c_v}$

$\Gamma$ $\left(\frac{1}{\gamma}\right)^{\frac{1}{2\beta}} \left(\frac{\gamma + 1}{2}\right)^{\alpha}$

$\lambda$ yaw angle

$\mu$ coefficient of viscosity

$\rho$ density

Subscripts

b body conditions

r reflected shock

s incident shock

t stagnation conditions

$\infty$ conditions in the free stream

$\lambda$ yaw angle

## EXPERIMENT

### Test Apparatus

An apparatus has been developed in which heat transfer to aerodynamic shapes can be measured in a steady-state hypersonic air stream at the same temperature potentials which occur in high-speed flight. This apparatus is shown in figure 1. The design criteria for this apparatus were established by the method discussed in appendix A. A brief description of this equipment and its calibration will be given here.

Description.- A schematic diagram of the test apparatus is shown in figure 2. A light gas (helium) is stored in the compressor chamber at high pressure and is separated from the low-pressure air in the pump tube by a copper diaphragm. Shock compression in the pump tube is initiated when the diaphragm is pierced by a punch. The incident shock traverses the pump tube to the nozzle where it is reflected back toward the compressor chamber. In appendix A it is shown that the gas flow into

the pump tube can be regulated so that a one-cycle shock process results. This is accomplished by the perforated plates in the inlet to the pump tube which throttle the flow of the helium into the pump tube to establish the shock strength required for equilibrium at the contact surface between the helium and the air. The perforated plates also attenuate the reflected shock as it comes back to the compressor chamber. If the reflected shock is so attenuated, no further disturbances are propagated into the pump tube. The high-pressure, high-temperature air produced at the end of the pump tube is then at rest in a reservoir of about 5 percent of the total length of the pump tube. This air is expanded through the nozzle to provide a high-velocity test stream with a high stagnation temperature. The advantages of producing the high-temperature reservoir of air with a one-cycle shock compression are discussed in appendix A. These include the elimination of pressure and temperature fluctuations produced by multiple shock reflections and the elimination of disadvantages inherent in such fluctuations. In addition, from the instant the primary shock is reflected from the nozzle end of the pump tube a hot hypersonic air stream is generated with sufficient duration that heat-transfer measurements can be made in a steady-state flow field.

For the tests described in this report, helium was stored in the compressor chamber at 1665 pounds per square inch absolute and at room temperature. The chamber (see fig. 1) has a 5-inch bore diameter and a volume of approximately 1000 cubic inches. For these tests, a diaphragm of 0.019-inch-thick annealed copper separated the compressor chamber and the pump tube. In figure 3 are shown a diaphragm before installation and one that has been ruptured. Rupture of the diaphragm was started by the punch shown in figure 4. This punch was actuated by an electrically ignited powder charge. The relative alinement of the punch and the diaphragm is shown in figure 5. In this figure are also shown the perforated plates with which the flow into the pump tube was controlled. A more detailed schematic view of the inlet section (fig. 6) shows the holes in the center of the plates through which the punch was guided to pierce the diaphragm. The plates were 24-gage commercial stainless steel having holes of 0.045-inch diameter with 27-percent open area. Two such plates, spaced as shown in figure 6, were used for this experimental program.

The pump tube (see fig. 1) consists of a 20-mm smooth-bore barrel 5 feet long. It is secured to the compressor chamber by a flange in which the inlet assembly (fig. 6) is installed. For these tests, the pump tube was initially charged with dry air at 12 psia. The end opposite the diaphragm is fitted into the reservoir block, shown in figure 1, in which a piston-operated resistance strain gage is installed.

The nozzle (fig. 7(a)) is fitted to the reservoir block in line with the pump tube (fig. 1). The inlet and sonic throat section are machined as an insert which can be replaced (see fig. 7(b)). Inserts with 0.040-, 0.063-, and 0.094-inch-diameter sonic throats are provided. The nozzle has a simple conical contour of 9° total angle with a 2-inch exit diameter.

Although the flow is thus expanding conically, in the region of the models the rate of expansion is slow and for most practical purposes the flow can be considered uniform.

The 2- by 2-inch test section, shown in figure 1, is 14 inches long. Since models are mounted in the test region (see fig. 2) where the Mach number is not affected by the shape of the test section, no attempt need be made to provide for flow transition from the conical nozzle to the square test section. The flow from the test section passes through a simple diverging diffuser into a 10-cubic-foot vacuum tank. An adhesive-backed film diaphragm covers the inlet to the nozzle to provide a seal between the pump tube and the test section. Thus, the nozzle, test section, and vacuum tank can be evacuated to pressures less than 0.1 mm of mercury. This provides compression ratios which are high enough to maintain hypersonic flow in the test section until all the air in the reservoir is expanded through the nozzle. Evacuation to pressures below 0.1 mm of mercury is also necessary to prevent shock-heating of air in the nozzle at the start of flow, since air so heated causes noticeable spurious initial temperatures on heat-transfer models.

Calibration.- Properties of the test stream were determined from measurements of reservoir pressure, pitot pressure, and stream velocity. It should be noted that the calibration of the test region did not include static-pressure measurements. However, it will be seen later that the static-pressure measurements are not needed for relating the experimental heat-transfer parameters used in this report to the stream properties.

Reservoir pressures for each test were measured from the side of the reservoir block with the strain-gage unit shown in figure 1. The gage and its operation have been described in reference 1. In addition, reservoir pressures were measured at the nozzle end of the pump tube with a quartz-crystal piezoelectric pressure transducer with a 48-kilocycle natural frequency. The transducer was mounted in the reservoir block in the position to be used later for the nozzle. The pressure-induced output of the transducer was passed through a calibrator-attenuator into an oscilloscope. The sweep of the oscilloscope was triggered by the same electrical impulse which ignited the powder charge of the punch. Thus, a continuous record was taken of the reservoir pressure from the instant the punch was actuated. Typical photographic records of the outputs of the strain-gage unit and the piezoelectric transducer are shown in figures 8 and 9.

The reservoir pressure records were also used to determine conditions required for total equilibrium after one-cycle shock compression. The conditions included the spacing, geometry, and number of perforated plates needed to control the flow of helium into the pump tube. Shown in figure 8 are two records of reservoir pressure fluctuations which occur when no plates are used for throttling. Similar fluctuations occurred when throttling with plates was only partially effective. Shown

in figure 9 are two pressure records for the throttling arrangement selected as the most effective. In figure 9(a), the record shows a pressure jump to within 10 percent of the final pressure at the instant the primary shock was reflected from the end of the pump tube. The final pressure was reached in less than 2 milliseconds and thereafter did not differ from the equilibrium pressure by more than ±5 percent. This indicates that the contact surface between the helium and the air had been brought essentially to rest with respect to the pump tube by the interaction with the reflected shock, and that the reservoir air was disturbed only by minor pressure waves. These minor fluctuations in reservoir pressure are shown in figure 9(b) to decay to half their initial amplitude in less than 10 milliseconds. Essentially, then, the reservoir pressure remained constant at 1615 psia from the moment the incident shock wave was reflected from the end of the pump tube.

The pitot pressure was measured with a conventional strut-mounted probe. The 0.040-inch-diameter sonic throat was used for these tests. A photograph of the test section with the pitot probe installed is shown in figure 10. The 0.065-inch O.D., 0.050-inch I.D. probe was supported by a 5° included-angle wedge with a sharp leading edge and the piezoelectric transducer used for the reservoir pressure measurements was mounted in the supporting strut. The calibrator-attenuator previously mentioned in conjunction with the transducer is also shown in the photograph. Two pitot-pressure records are shown in figure 11. The oscillations are believed to be due to the internal flow characteristics of the pitot probe. Since the reservoir pressure was constant the pitot pressure was deduced to be constant and was taken to be the mean value of the trace shown in figure 11(a). Since it was known that the reservoir pressure jump was essentially instantaneous (see fig. 9), it can be judged that the pitot pressure probably reached an equilibrium value of 2.2 psia in less than the 2 milliseconds indicated by the record of figure 11(b).

The stream velocity was determined by means of the technique discussed in reference 1. Briefly, a disturbance is produced by a high-voltage spark discharge between the electrodes shown in figure 12. As the disturbance passes through the test section, its position is recorded photographically by a schlieren apparatus. The time of travel is the time interval between the discharge of the disturbance spark and the discharge of the spark light source of the schlieren apparatus. From the location of the centers of the disturbance in the schlieren photograph (see fig. 13), the distance traveled from the tips of the electrodes can be determined. Thus, the average velocity can be determined by dividing the distance traveled by the time interval of travel. Measurements of velocity were made in separate tests over a range of times from 2 to 90 milliseconds after the start of flow. In figure 14 it can be seen that the velocity is constant at 6500 feet per second for the first 50 milliseconds of flow with deviations of only ±100 feet per second. Note that the velocity data are for the 0.063- and 0.094-inch-diameter sonic throats. The schlieren photographs of the air flow for the tests in which the

0.040-inch diameter sonic throat was used lacked sufficient detail for accurate location of the centers of the disturbances. Note, however, that the stream velocity in hypersonic flow does not change appreciably with Mach number, increasing, for example, by only 2 percent from M = 10 to 12. As will be seen, this is within the Mach number range of these tests. Therefore, it is within the accuracy of the experiments to assign the 6500-foot-per-second air-stream velocity to the tests in which the 0.040-inch-diameter sonic throat was used. With the stream velocity and pitot pressure known, an estimate was made, using ideal-gas equations, of the stagnation temperature and stream density. The time required for the stream to reach chemical equilibrium was calculated from relaxation times given by Logan (ref. 8). The calculations indicated that the stream should reach equilibrium within the nozzle. Therefore, stream properties presented in this report have been evaluated for air in chemical equilibrium. Furthermore, the heat-transfer parameters presented herein deviate by not more than 5 percent from those estimated from real-gas properties presented by Hansen (ref. 9).

The stream properties needed to determine the aerodynamic parameters include the density and the total temperature. The reservoir pressure was not used directly to determine these properties but was used to determine an approximate pitot-pressure Mach number. From the ratio of measured pitot pressure to measured reservoir pressure, $p'/p_t = 1.4\times10^{-3}$, the pitot-pressure Mach number with the 0.040-inch-diameter sonic throat and $\gamma = 1.4$ was found to be approximately 11.8. Since the true Mach number is usually somewhat lower than the pitot-pressure Mach number, a second method was used to estimate the Mach number range. The schlieren photographs shown in figure 15 are of flow over the pitot-pressure probe. The shock from the end of the semispan strut can be seen in each photograph. Since downstream of the strut the shock wave angle is approximately equal to the Mach angle, the Mach number of flow can be estimated from these shock waves. The Mach number was estimated from shock-wave angles, for $\gamma = 1.4$, to be 9.5 for the 0.094-inch-diameter sonic throat and 10.4 for the 0.063-inch-diameter sonic throat. A shock wave was discernible in a photograph of flow with the 0.040-inch-diameter sonic throat but lacked sufficient detail to be measured. It is likely, however, that the true Mach number for this sonic throat should be higher than the true Mach number for the 0.063-inch-diameter sonic throat. Thus, the true Mach number of flow with the 0.040-inch-diameter sonic throat is undoubtedly between 10.4 and 11.8, the pitot-pressure Mach number. Now, the heat-transfer-rate comparisons made in this report do not depend on Mach number of flow; therefore, it is sufficient for reference purposes to state that these data were taken at a nominal Mach number of 11.

At hypersonic Mach numbers, the ratio of pitot pressure $p'$ to dynamic pressure $q_\infty$ is approximately independent of Mach number; namely,

$$\frac{p'}{2q_\infty} = \frac{p'}{\rho_\infty u_\infty^2} \equiv \Gamma(\gamma) \equiv \left(\frac{1}{\gamma}\right)^{\frac{1}{2\beta}} \left(\frac{\gamma + 1}{2}\right)^{\alpha} \qquad (1)$$

Since $\Gamma(\gamma)$ is very nearly constant, varying, for example, from 0.920 to 0.935 as $\gamma$ varies from 1.4 to 1.3, the stream density $\rho_\infty$ can be calculated from measured properties $p'$ and $u_\infty$:

$$\rho_\infty = \frac{p'}{\Gamma u_\infty^2} \tag{2}$$

The stream density was assumed constant during the test interval consistent with the constant value of velocity and of the pitot pressure, and was calculated to be $7.9\times10^{-6}$ slugs per cubic foot from the value of 2.2 psia for the pitot pressure and $\gamma = 1.4$.

The stagnation temperature, $T_t$, is calculated from a form of the integrated energy equation

$$T_t = \frac{u_\infty^2}{2c_p\left(1 - \frac{T}{T_t}\right)} \tag{3}$$

The term $(1 - T/T_t)$ is a very weak function of Mach number in hypersonic flow equations; therefore, its evaluation at exactly the true Mach number is not necessary. Since the velocity of the stream was found to be constant, the stagnation temperature was deduced to be constant and was calculated to be $3660^\circ$ R for $c_p = 6.0\times10^3$ ft-lb/slug $^\circ$R. This stagnation temperature will be used along with the stream density and velocity to provide a basis for relating Nusselt number with Reynolds number in a manner which is relatively independent of Mach number (ref. 3). Since the stagnation-point mass flow equals the free-stream mass flow according to mass conservation requirements, a stagnation Reynolds number can be computed from free-stream density and velocity and the coefficient of viscosity evaluated at stagnation conditions. This stagnation Reynolds number was found to be $4.0\times10^4$ per foot with $\mu_t = 1.3\times10^{-6}$ slug/ft sec (the free-stream Reynolds number corresponding to flow at the nominal Mach number of 11 would be $5.2\times10^5$ per foot with $\mu = 1.0\times10^{-7}$ slug/ft sec).

The purity of the air stream was also investigated. Since the helium in the pump tube could possibly mix with the air, an optical detector was developed to indicate qualitatively the presence of helium in the test stream. A schematic diagram of this helium detector is shown in figure 16. A continuous corona discharge at the spark electrodes ionizes the test stream. A photomultiplier is fitted with an interference filter which will pass only the prominent helium lines of 5875 Å. The electrical output of the photomultiplier is fed into a recording oscilloscope. A typical photographic record of the output is shown in figure 17. The presence of helium in detectable quantities begins approximately 40 milliseconds after the start of flow. Model surfaces were examined optically after each test for the presence of solid phase impurities; no such impurities were detected.

## Heat-Transfer Models and Reduction of Data

The models used in the heat-transfer experiments were butt-welded iron-constantan thermocouple cylinders of 0.003-, 0.012-, and 0.020-inch diameter. These were chosen because iron and constantan have nearly equal thermal capacities. Thus, the weld junctions were representative of a cross section of a homogeneous cylinder. The cylinders were examined microscopically, and those used showed no visible imperfections at the welded junction. The cylinders spanned the test section with the junction on the stream center line. They were tested normal to the flow (zero yaw) and at 22.5°, 45°, and 70° angle of yaw. A typical installation, a 0.020-inch-diameter cylinder at 45° angle of yaw, is shown in figure 18. It should be noted that although the 0.063- and 0.094-inch-diameter sonic throats were used to obtain stream velocity data, only the 0.040-inch-diameter sonic throat was used for heat-transfer measurements.

Heat-transfer parameters were deduced from measured rates of the change of cylinder temperature by the method of reference 1. Temperature gradients across the thermocouple junction and along the cylinder were assumed to be negligible. Under these conditions the average rate of heat transfer per unit area to the models is proportional to the rate of change of temperature indicated by the thermocouple junction. Thus, the average heat-transfer rate satisfies the relation

$$Q = \frac{r_b c_b \rho_b}{2} \frac{dT_b}{dt} \tag{4}$$

where $dT_b/dt$ is the rate of change of temperature of the cylinder with a radius $r_b$, specific heat $c_b$, and density $\rho_b$.

For cylinders at zero yaw, an average heat-transfer coefficient is defined by the equation

$$\bar{h} = \frac{Q}{T_t - T_b} \tag{5}$$

wherein $T_t$ is the total temperature of the stream and $T_b$ is the cylinder temperature at the beginning of flow. Then the average Nusselt number $\overline{Nu}$, based on stagnation temperature conditions ($k_t = 1.95 \times 10^{-5}$ Btu/sec ft °R) and a characteristic length equal to the diameter of the cylinder, is given by the equation

$$\overline{Nu} = \frac{2\bar{h} r_b}{k_t} = \frac{r_b^2 c_b \rho_b}{k_t (T_t - T_b)} \frac{dT_b}{dt} \tag{6}$$

The effect of yaw on the aerodynamic heating of a circular cylinder has been treated by comparing rates of change of temperature measured at yaw with rates measured at zero yaw. The ratio of average heat-transfer rates is given by the equation

$$\frac{Q_\lambda}{Q_{(\lambda=o)}} = \frac{(dT_b/dt)_\lambda}{(dT_b/dt)_{\lambda=o}} \tag{7}$$

A typical temperature-rise record is shown in figure 19(a). Since the initial temperature rise was of principal interest, oscilloscope sweep speeds were adjusted to give a slope of the temperature time curve of approximately 45° whenever possible. The record shown includes the first 8 milliseconds of flow. The rate of temperature rise for this run was determined to be 51,600° R per second.

It was previously noted that pressure records were used to evaluate the effectiveness of the throttling plates. Temperature-rise records were also used for this evaluation. The record shown in figure 19(b) was taken with a 0.003-inch-diameter cylinder at zero yaw. For this run, no throttling plates were used. The changes in heating rate indicated by the waviness of the trace correspond in time with the pressure fluctuations of figure 8. Note that such waviness is hardly detectable on the trace of figure 19(a). This was interpreted as evidence that the stagnation pressure fluctuations indicated by the records of figure 9 do not influence aerodynamic heating rates.

## RESULTS AND DISCUSSIONS

### Experimental Results

Average heat-transfer rates have been calculated from rates of temperature rise of circular cylinders tested. These cylinders were tested normal to the air stream (zero yaw) and at various angles of yaw. The data obtained at zero yaw are presented in figure 20(a) along with the data of references 1, 4, 5, and 6. Specifically, there are shown average Nusselt numbers as a function of the reciprocals of stagnation Reynolds numbers. It should be noted that there is a large difference in test conditions at which the various data were taken. For example, the data of Stine (ref. 6) are for Mach numbers less than 1.4 with stagnation temperatures less than 590° R. Nevertheless, the agreement between the present data and the earlier data is reasonably good.

The same data are presented in the manner of Stalder, Goodwin, and Creager (ref. 4) in figure 20(b). In this figure are shown average Nusselt numbers as a function of stagnation Reynolds numbers. The Nusselt numbers from the present tests were found to be proportional to the 0.65 power of the stagnation Reynolds numbers. However, it was shown experimentally in reference 1 that, in high Mach number flow, Nusselt numbers are proportional to the square root of the stagnation Reynolds numbers. This is essentially the result deduced experimentally by Kovaznay and Tormarck (ref. 5) and by others for average Nusselt numbers of cylinders transverse

to subsonic and low Mach number supersonic continuum flows. On the other hand, in reference 4, experimental values for Nusselt numbers in rarefied gas flow were reported to be proportional to the 3/4 power of stagnation Reynolds numbers.

Consideration of the flow Knudsen numbers may account for the observed differences in the exponential relationship of the Nusselt numbers and stagnation Reynolds numbers for the various investigations. If the exponent should be one-half for fully developed continuum flow and should approach unity for free-molecule flow, it is likely that the exponent would lie between unity and one-half in a slip-flow regime. It was shown in reference 4 that noncontinuum flow occurs at Knudsen numbers greater than 0.1. The Knudsen numbers of the cylinders of the present tests were calculated from nominal Mach numbers and Reynolds numbers to lie between 0.02 and 0.14. The relationship $Nu = 0.16\ Re_t^{0.65}$ (figs. 20(a) and 20(b)) followed by these experimental data may be consistent with a hypothesis that these data pertain to the domain between continuum and free-molecule flow.

The effect of yaw on the aerodynamic heating of a circular cylinder will now be considered. Experimentally determined heat-transfer reductions with increasing yaw are shown in figures 21 and 22 with the analytic curves, $Q_\lambda/Q_{(\lambda=0)} = \cos^{3/2}\lambda$. Note that for the data shown in figure 21 the scatter at 22-1/2° yaw angle is no more than ±2 percent. This represents an error in reading the initial slope of the temperature trace (fig. 19(a)) of no more than ±0.02 cm per cm. However, this limit in reading accuracy results in somewhat greater deviations at higher angles of yaw. Because of these deviations and because of the small Reynolds number range of these tests, it is not possible to determine the extent to which the reductions shown in figure 21 are influenced by Reynolds number.

There are shown in figure 22 data from references 1 and 7. Observe by comparing figures 21 and 22 that although the data from reference 1 and the present tests are for high Mach number flow, the present data show greater heat-transfer reductions at 70° yaw angle. This variation may be a result of the differences in model supports in the two investigations. In reference 1, the cylinder supports projected well into the test stream. In contrast, for the present tests the cylinders completely spanned the test section (see fig. 18) with no projecting supports. Thus, it is believed that the present heat-transfer data have been obtained in a more nearly two-dimensional flow field than was achieved in the tests of reference 1.

Observe by comparing figures 21 and 22 that heat-transfer reductions reported in reference 7 differ from those of the present tests. Note that the present tests were conducted with a body-to-stagnation temperature ratio of 0.14; whereas the temperature ratio of reference 7 was approximately 0.5. In addition, the fineness ratios of the cylinders in the present tests were over 100; whereas the fineness ratios of the cylinders of

reference 7 were 12. These two factors could account for the larger reductions in heat-transfer rates observed in the present tests.

## Comparison of Theory With Experiment

The predictions of heat-transfer rates to circular cylinders at yaw will now be considered. Theoretical methods for determining the influence of yaw on heat transfer to cylindrical stagnation regions have been given in references 1, 2, and 3. These theories can be compared with experiment if it can be established that measured average heat-transfer rates to solid circular cylinders are proportional to calculated stagnation-region heat-transfer rates. The theoretical considerations outlined in references 2 and 3 show that the average heat-transfer coefficient is proportional to the local heat-transfer coefficient when the local velocity at the boundary-layer edge is directly proportional to the azimuth angle. In reference 3, it was shown that this condition is also true for yawed cylinders if the Mach number is greater than about 2.5. This finding ($\bar{h} \sim h_{local}$) has been verified experimentally in reference 3 for $M = 3.9$.

The solutions given in reference 1 are for cases in which viscosity, thermal conductivity, and specific heat are arbitrary functions of temperature. These solutions include the following equation for predicting the effect of yaw on heat-transfer rates:

$$\frac{Q_\lambda}{Q_{(\lambda=0)}} = \frac{\cos^{\left(n+\frac{1}{2}\right)}\lambda}{1 - (T_b/T_t)^{n+1}} \left\{ \cos^2\lambda \left[ 1 - \left( \frac{T_b}{T_t \cos^2\lambda} \right)^{n+1} \right] + (n+1)\,Pr\,\frac{1}{2} \left[ 1 + \left( \frac{T_b}{T_t \cos^2\lambda} \right)^{n} \right] \sin^2\lambda \right\} \tag{8}$$

Reshotko and Beckwith (ref. 2) present equations for compressible laminar boundary-layer flow over a yawed infinite cylinder. These equations include the effects of heat transfer and arbitrary Prandtl number. Expressions are given for stagnation-line heat transfer and the variation of heat-transfer coefficient with yaw angle. The ratio of yawed to normal heat-transfer coefficient for a cylinder with the same conditions of free-stream and surface temperature appears to approach a limiting curve at Mach numbers greater than 7. This limiting ratio is given as

$$\frac{\eta_\lambda}{\eta_{(\lambda=0)}} = \frac{(\theta_w')_{t_o/t_{N_o}=\sec^2\lambda}}{(\theta_w')_{\lambda=0}} \cos^{3/2}\lambda \tag{9}$$

in the notation of reference 2. The yaw parameter $t_o/t_{N_o}$ is a local static temperature ratio relating Mach number and yaw angle, whereas $\theta_w'$ is the rate of change of a normalized enthalpy function evaluated at the wall.

The influence of yaw on the heat-transfer coefficient at the forward stagnation point of a cylinder has also been treated in reference 3. An expression was derived for the ratio of heat-transfer coefficients at yaw to the heat-transfer coefficient at zero yaw. This ratio of heat-transfer coefficients was presented as a function of yaw angle and Mach number. It may be noted that the ratio approaches a $\cos^{3/2}\lambda$ limit for $M = \infty$ and lies very close to this limit for Mach numbers in excess of 7.

Possible reductions in heating rates at angles of yaw have been calculated by the theories of references 1, 2, and 3. The method of reference 1 was used to treat two surface-to-stagnation temperature ratios, namely, $T_b/T_t = 0$ and $T_b/T_t = 0.14$. The latter value corresponds to the test conditions in the 2-inch hypervelocity wind tunnel. According to equation (8), the stagnation-region heat-transfer rates are influenced by yaw in the manner shown in figure 23. The Prandtl number was taken equal to three-fourths and the temperature exponent for the thermal conductivity and viscosity functions was taken as one-half. The method of reference 2 was used with equation (9) to calculate the effect of yaw on stagnation-line heat-transfer rates. The resulting curve shown in figure 23 includes the influence of variable Prandtl number and surface-temperature level as discussed in reference 2. Also shown in figure 23 is the $\cos^{3/2}\lambda$ curve previously noted as the limiting value of the equation derived in reference 3 for heat-transfer reductions due to yaw in very high Mach number flow.

How well these predicted reductions agree with the present data is seen by comparing figures 21 and 23. The data are observed to decrease with increasing yaw slightly more than the $\cos^{3/2}\lambda$. However, the experimental scatter is seen to be at least as much as the differences in the theoretical values shown in figure 23, with the exception of the $T_b/T_t = 0.14$ case at yaw angles greater than $50^\circ$. Therefore, it is not proper to select one theory as the most representative, but it is apparent that within the accuracy of the experimental data, reductions of the order of $\cos^{3/2}\lambda$ can be effected by yaw. Thus, a means for estimating possible reductions in average rates of heat transfer can be set up with the relationship $Q_\lambda/Q_{(\lambda=0)} = \cos^{3/2}\lambda$.

## CONCLUDING REMARKS

An apparatus has been developed in which heat-transfer rates can be measured in a 6500-foot-per-second hypersonic air stream for at least 40 milliseconds. Measured average rates of heat transfer to circular

cylinders normal to high-velocity air flow were found to be proportional to the 0.65 power of the stagnation Reynolds number. These heat-transfer rates were in good agreement with heat-transfer rates obtained in earlier experiments, including those obtained in considerably lower velocity flow. The value of the exponent, 0.65, leads one to conclude that these data may have been taken in a region of transition between continuum and free-molecule flow. Average rates of heat transfer to circular cylinders in high-velocity air flow were found to decrease with increasing yaw angle, $\lambda$, about as $\cos^{3/2}\lambda$. These reductions in average heat-transfer rate agree reasonably well with reductions which are predicted with stagnation-region heat-transfer theory.

Ames Aeronautical Laboratory
National Advisory Committee for Aeronautics
Moffett Field, Calif., May 19, 1958

# APPENDIX A

## ANALYSIS OF ONE-CYCLE SHOCK PROCESS

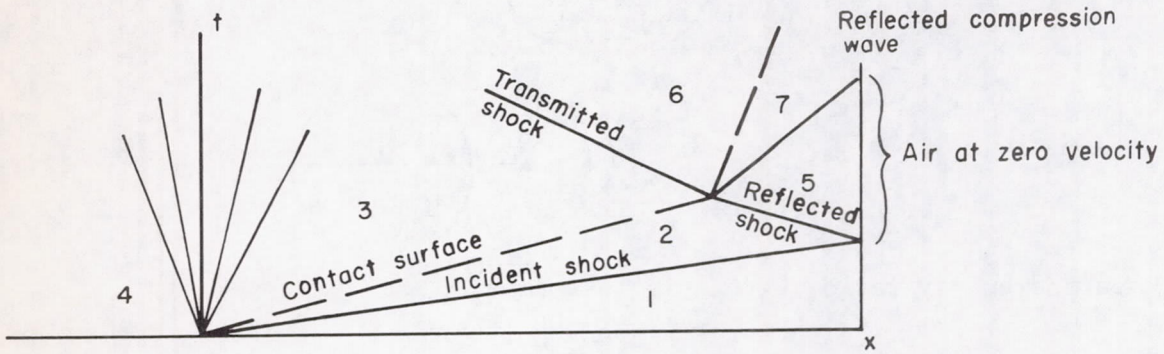
One of the problems associated with simulation of aerodynamic heating of hypervelocity vehicles is the generation of an air stream with which flight velocities and Reynolds numbers can be duplicated. One technique, shock compression of air in shock tubes, has been used extensively to generate high Mach number flows. This process has been reported by Glass and Patterson (ref. 10), Hertzberg, Smith, Glick, and Squire (ref. 11), Dosanjh (ref. 12), and by several others. For high Mach number flow, testing times are of the order of 0.01 millisecond per foot of shock-tube length (ref. 11). However, testing times with high Mach number flow are limited by the rapidly changing stream properties due to marked attenuation of the incident shock wave. Such attenuation was reported by Hertzberg (ref. 13), for example. Because of this attenuation, flow time cannot be increased merely by the use of longer shock tubes. If an attempt were made to compensate for the attenuation with stronger incident shocks, the density, and thus the Reynolds number of flow, would be lower because of practical limits on compressor chamber pressures.

Longer flow times can be realized, however, if the incident shock wave is reflected from the end of the shock tube. In this process, the air in the shock tube is compressed into a high-temperature reservoir and can be expanded through a nozzle into a conventional wind-tunnel-type test section. One such device, reported in reference 1, was used with an exploding powder charge and valving system to provide testing times up to one second, with stream stagnation pressures and temperatures up to 4500 pounds per square inch and 2200° R. In the operation of that equipment at higher equilibrium temperatures and pressures, the excessive pressure and temperature peaks produced by the exploding powder charge eroded the reservoir and nozzle surfaces. This resulted in damaged equipment and contaminated air in the test stream. It was decided to modify this equipment, retaining the reflected-shock compression technique but eliminating, if possible, the use of an exploding powder charge and valving system.

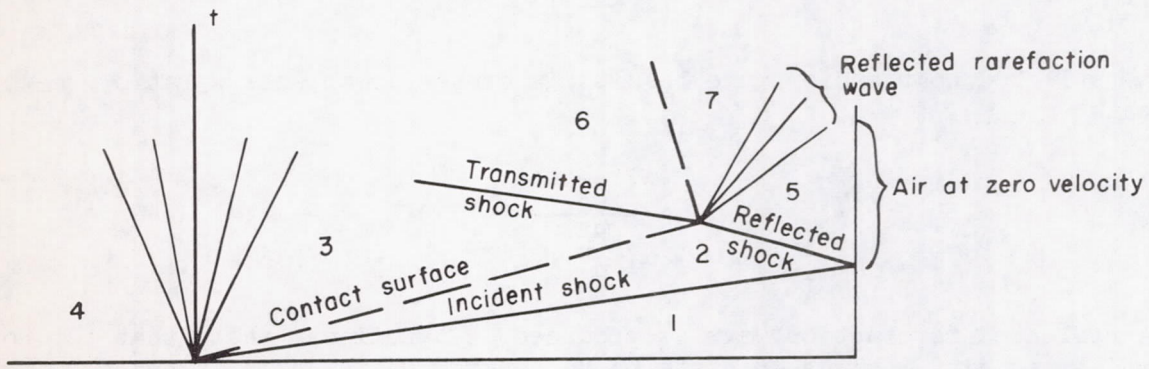
It has been established (see ref. 10, for example) that a light gas in the compressor chamber of a shock tube can be used to produce strong shocks in air. Thus, an energy source equivalent to an exploding powder charge is available for shock compression. When a nozzle is incorporated in the closed end of a shock tube and is used without a valving system, a test stream is generated as soon as the incident shock is reflected from the end of the shock tube. However, when no valve system is used, testing times may be limited by reflected pressure waves disturbing the reservoir air. It would be desirable, then, to provide shock compression with a one-cycle shock process so that pressure and temperature

fluctuations can be eliminated. If no disturbances are reflected into the reservoir of air, flow times would be limited only by the mass of air in the reservoir and the flow rate through the nozzle. With such a process the air in the reservoir would be at zero velocity after compression by the reflected shock. This should minimize erosion of the reservoir surfaces by the scrubbing action of moving, high-temperature, high-pressure air. The following analysis is concerned with the feasibility of the generation of a hypervelocity air stream with one-cycle shock compression of air in a closed-end shock tube, or pump tube.

A wave diagram of the reflected shock system showing a reflected compression wave which disturbs the air at rest in state 5 is shown in sketch (a), while a reflected rarefaction wave is shown in sketch (b).




Sketch (a)




Sketch (b)

It should be noted that if the nozzle throat diameter is much less than the pump-tube diameter, air flow through the nozzle has a negligible effect on the strength of the reflected shock. In addition, this air flow will not influence the pressure of the air in state 5. Therefore, air flow through the nozzle need not be represented on the wave diagram. The flow time with constant stagnation pressure, when these disturbances are present, is of the order of 0.1 millisecond per foot of pump-tube

length for high incident shock strengths. An analysis of shock phenomena has shown that these disturbances can be eliminated when a light-gas driver is used. Thus, if there are no reflected disturbances, the contact surface will be at equilibrium (zero velocity) and the pressure ratio $p_7/p_5$ will be unity. It was shown in reference 10 that the character of these disturbances depends on the energy of the gases in states 2 and 3, shown in sketches (a) and (b). The energy ratio $e_3/e_2 = (c_vT)_3/(c_vT)_2$ appears in the equation

$$\frac{p_7}{p_5} + \left(\frac{\alpha_1 + \frac{p_2}{p_5}}{\alpha_1 \frac{p_2}{p_5} + 1}\right)^{\frac{1}{2}} \left(\frac{p_7}{p_5} - \frac{p_2}{p_5}\right) \left(\frac{\beta_1 \frac{e_3}{e_2}}{\alpha_4 \frac{p_7}{p_5} + \frac{p_2}{p_5}}\right)^{\frac{1}{2}} - \left(1 - \frac{p_2}{p_5}\right) \left(\frac{\beta_1}{\alpha_1 \frac{p_2}{p_5} + 1}\right)^{\frac{1}{2}} - 1 = 0 \qquad (A1)$$

When the energy ratio $e_3/e_2$ is less than

$$\frac{\alpha_4 \frac{p_5}{p_2} + 1}{\alpha_1 \frac{p_5}{p_2} + 1}$$

a reflected compression wave results; whereas for an energy ratio greater than

$$\frac{\alpha_4 \frac{p_5}{p_2} + 1}{\alpha_1 \frac{p_5}{p_2} + 1}$$

a reflected rarefaction wave is produced. It follows, then, that for no reflected disturbances in state 5, the energy ratio $e_3/e_2$ must be, for a pressure ratio $p_7/p_5 = 1$,

$$\frac{e_3}{e_2} = \frac{\alpha_4 \frac{p_5}{p_2} + 1}{\alpha_1 \frac{p_5}{p_2} + 1} \qquad (A2)$$

Now, the rate at which the driver gas flows into the pump tube controls the incident shock strength as well as the energy ratio $e_3/e_2$ and thus has an influence on equilibrium at the contact surface. Ideally,

equilibrium will occur at different shock strengths for different inlet areas (for the same initial energy ratio and pump tube cross-sectional area). Since the pressure in state 5 depends only on the shock strength, under certain conditions this pressure will be equal to the final pressure in the compressor chamber. In addition, while traversing the pump tube, the reflected shock is weakened by interaction with the forward moving rarefaction wave. If the attenuation of the reflected shock is complete, no appreciable disturbances will be transmitted into the pump tube when the reflected shock enters the compressor chamber.

Thus, with matched final pressures and no reflected disturbances at the contact surface or inlet section, the gases at all stations will be at the same pressure and at zero velocity. This condition of total equilibrium results in a one-cycle shock process. Thus, the air in state 5 will be at constant pressure and temperature after the incident shock has been reflected from the end of the pump tube. Since the properties of the air in state 5 depend only on the initial conditions in the pump tube and the incident shock strength, these properties can be determined with the general shock tube equations (see ref. 10, for example). The calculation of the initial conditions required for total equilibrium is an iterative procedure. For this report, these calculations are based on ideal gas relationships.

Note that the limiting shock strength for $e_1/e_4 \leqq 1$ is

$$\left(\frac{p_2}{p_1}\right)_{p_1/p_4=0} \approx 1 + \left(\frac{\alpha_1}{\beta_4}\right)\left(\frac{e_4}{e_1}\right) \tag{A3}$$

Thus, the temperature, pressure, and velocity ratios are computed:

$$\frac{T_2}{T_1} = \frac{\frac{p_2}{p_1}\left(\alpha_1 + \frac{p_2}{p_1}\right)}{1 + \alpha_1 \frac{p_2}{p_1}} \tag{A4}$$

$$\frac{p_5}{p_2} = \frac{\left(\alpha_1 + 2\right)\frac{p_2}{p_1} - 1}{\frac{p_2}{p_1} + \alpha_1} \tag{A5}$$

$$\frac{p_5}{p_1} = \left(\frac{p_5}{p_2}\right)\left(\frac{p_2}{p_1}\right) \tag{A6}$$

$$\frac{T_5}{T_2} = \frac{\frac{p_5}{p_2}\left(\alpha_1 + \frac{p_5}{p_2}\right)}{1 + \alpha_1 \frac{p_5}{p_2}} \tag{A7}$$

$$\frac{T_5}{T_1} = \left(\frac{T_5}{T_2}\right)\left(\frac{T_2}{T_1}\right) \tag{A8}$$

$$\frac{u_s}{a_1} = \left[\beta_1 \left(1 + \alpha_1 \frac{p_2}{p_1}\right)\right]^{\frac{1}{2}} \tag{A9}$$

$$\frac{u_2}{a_1} = \frac{\frac{p_2}{p_1} - 1}{\gamma_1 \left[\beta_1 \left(\alpha_1 \frac{p_2}{p_1} + 1\right)\right]^{\frac{1}{2}}} = \frac{\frac{p_2}{p_1} - 1}{\gamma_1}\left(\frac{a_1}{u_s}\right) \tag{A10}$$

$$\frac{u_r}{a_1} = \frac{2\frac{p_2}{p_1} + \alpha_1 - 1}{\left[\left(\alpha_1 + 1\right)\left(\alpha_1 \frac{p_2}{p_1} + 1\right)\right]^{\frac{1}{2}}} \tag{A11}$$

The contact surface, when brought to rest by the interaction with the reflected shock, will be a distance $X_{cs}$ from the diaphragm. This distance, per foot of pump tube, is

$$\frac{X_{cs}}{l} = 1 - \left(\frac{T_5}{T_1}\right)\left(\frac{p_1}{p_5}\right) \tag{A12}$$

Now, for no reflected disturbances at the interaction of the reflected shock and the contact surface, it is required that the energy ratio $e_3/e_2$ be given by equation (A2). For equilibrium in the compressor chamber the initial pressure $p_4$ must be such that the final pressure after one-cycle shock compression is equal to the reservoir pressure $p_5$. To get total equilibrium, a finite volume compressor chamber must be used with suitable throttling at the inlet to the pump tube to produce a shock system which will satisfy equation (A2). The analysis concerning the effect of inlet area ratio on shock strength and equilibrium at the contact surface is given in appendix B. It was found that for total equilibrium, inlet flow should be throttled to simulate an effective inlet area ratio of 1.

To continue with the determination of initial conditions required for total equilibrium, the initial energy ratio, for an effective inlet area ratio of one ($A_4/A_1 = 1$) is

$$\frac{e_4}{e_1} = \left[ \left( \frac{T_2}{T_1} \right) \left( \frac{e_3}{e_2} \right)^{\frac{1}{2}} + \left( \frac{p_2}{p_1} - 1 \right) \left( \frac{\beta_4}{1 + \alpha_1 \frac{p_2}{p_1}} \right)^{\frac{1}{2}} \right]^2 \tag{A13}$$

From this energy ratio, the initial temperature and pressure ratios for each value of incident shock strength can be determined. The temperature ratio is

$$\frac{T_4}{T_1} = \frac{m_4(\gamma_4 - 1)}{m_1(\gamma_1 - 1)} \frac{e_4}{e_1} \tag{A14}$$

The pressure ratio is

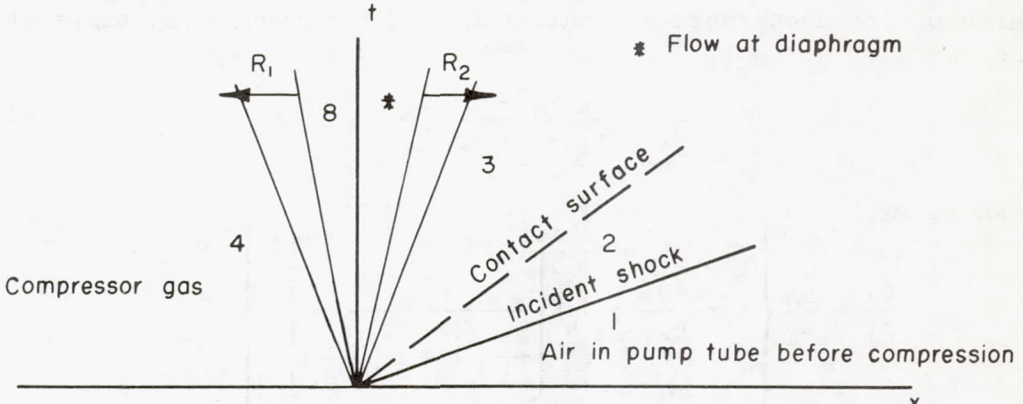
$$\frac{p_4}{p_1} = \frac{p_2}{p_1} \left\{ 1 - \left( \frac{p_2}{p_1} - 1 \right) \left[ \frac{\beta_4}{\frac{e_4}{e_1} \left( 1 + \alpha_1 \frac{p_2}{p_1} \right)} \right]^{\frac{1}{2}} \right\}^{-\frac{1}{\beta_4}} \tag{A15}$$

The shock strength corresponding to a given temperature ratio is determined by iteration from equation (A13). The initial pressure ratio can be determined with equation (A15) at this shock strength. Equations (A1) through (A15), then, can be used to calculate the initial conditions required to provide a shock system with no reflected disturbances at the interaction of the reflected shock and the contact surface. This system, together with the throttling technique discussed in appendix B, will produce a reservoir of air at equilibrium pressure and temperature. This air can be expanded through a nozzle to provide testing times from 10 to 100 times longer than would be possible if there were no equilibrium at the contact surface.

## APPENDIX B

## CONTROL OF FLOW INTO PUMP TUBE

The strength of the incident shock in a shock tube depends on the inlet area ratio as well as the initial energy and pressure ratios. It was shown by Glass, Martin, and Patterson (ref. 14) that the shock strength can be determined for inlet area ratios from 1 to infinity. The equations used in this appendix were derived from expressions given in reference 14. Inlet flow is represented schematically with the wave diagram shown in sketch (c).




Sketch (c)

If the initial conditions are such that behind the contact surface $M_3 > 1$, then sonic velocity is reached at the diaphragm. Then, with

$$\frac{A_4}{A_1} = \frac{A_4}{A_*} = \frac{1}{M_8}\left[\frac{2 + (\gamma_4 - 1)}{\gamma_4 + 1} M_8^2\right]^{\frac{\alpha_4}{2}} \tag{B1}$$

the pressure ratio $p_8/p_*$ is

$$\frac{p_8}{p_*} = \left[\frac{\gamma_4 + 1}{2 + (\gamma_4 - 1)M_8^2}\right]^{\frac{1}{2\beta_4}} \tag{B2}$$

The pressure ratio for a rarefaction wave $R_1$ which accelerates the gas from rest to $M_8$ is given by the unsteady flow equation

$$\frac{p_4}{p_8} = \left(1 + \frac{\gamma_4 - 1}{2} M_8\right)^{\frac{1}{\beta_4}} \tag{B3}$$

Finally, to reach $M_3 > 1$, a second rarefaction wave $R_2$ is required such that

$$\frac{p_*}{p_3} = \left[\frac{2 + (\gamma_4 - 1)M_3}{\gamma_4 + 1}\right]^{\frac{1}{\beta_4}} \tag{B4}$$

Thus for a known inlet area ratio, when $M_3 > 1$, the over-all pressure ratio across the rarefaction waves (and diaphragm) is given by

$$\frac{p_4}{p_3} = \left(\frac{p_4}{p_8}\right)\left(\frac{p_8}{p_*}\right)\left(\frac{p_*}{p_3}\right) \tag{B5}$$

With $p_3 = p_2$, it is desired to select the incident shock for which there are no reflected disturbances when the reflected shock interacts with the contact surface. This condition is satisfied when

$$M_3 = \frac{u_3}{a_3} = \left(\frac{u_2}{a_1}\right)\left(\frac{a_1}{a_2}\right)\left[\frac{\gamma_1(\gamma_1 - 1)}{\gamma_4(\gamma_4 - 1)}\frac{e_2}{e_3}\right]^{\frac{1}{2}} \tag{B6}$$

and the energy ratio $e_2/e_3$ has been computed according to equation (A2)

$$\frac{e_3}{e_2} = \frac{\alpha_4 \dfrac{p_5}{p_2} + 1}{\alpha_1 \dfrac{p_5}{p_2} + 1}$$

Since $M_3$ differs for each value of incident shock strength $p_2/p_1$, the pressure ratio $p_4/p_3$ will be different for each shock strength for each inlet area ratio chosen. By iteration, the initial pressure ratio $p_4/p_1$ can be calculated for each inlet area ratio, since

$$\frac{p_4}{p_1} = \left(\frac{p_4}{p_2}\right)\left(\frac{p_2}{p_1}\right) \tag{B7}$$

Now, the shock strength $p_2/p_1$ required for equilibrium at the contact surface will be set by the initial temperature ratio $T_4/T_1$. This shock strength can be determined by iteration for a known temperature ratio and inlet area ratio with

$$\frac{T_4}{T_1} = \frac{e_3}{e_2}\left(\frac{T_4}{T_3}\right)\left(\frac{T_2}{T_1}\right)\frac{(\gamma_4 - 1)m_4}{(\gamma_1 - 1)m_1} \tag{B8}$$

$$\frac{T_4}{T_3} = \left(\frac{p_4}{p_3}\right)^{2\beta_4} \tag{B9}$$

For total equilibrium, the final air pressure in state 5 must be equal to the final gas pressure in the compressor chamber. The pressure ratio $p_4/p_5$ is determined by iteration using equations (A2) to (A15) and equations (B1) to (B9). For equilibrium at the contact surface, it is found that this ratio is approximately constant for each inlet area ratio, regardless of shock strength. This means that for a given temperature ratio and inlet area ratio there is but one shock strength with which equilibrium at the contact surface can be produced. Since the final pressure in a finite volume compressor chamber will be less than the initial pressure, $p_4$, because of gas flow into the pump tube, a shock strength must be chosen that will result in a final air pressure less than $p_4$. It is found that the pressure ratio will be only slightly greater than one for an inlet area ratio of 1 with a helium to air drive and an initial temperature ratio $T_4/T_1$ equal to 1. If the compressor chamber diameter is larger than the pump tube diameter, the flow into the pump tube must be controlled to produce an inlet area ratio that effectively is unity. This can be done by throttling the flow with a set of porous plates. To be effective, throttling should reduce the inlet flow velocity to a value consistent with $M_3$ calculated with equation (A6). Whereas some analytical work has been done relating flow velocity to screen porosity (see ref. 15, for example), the porous plates used in the present apparatus were selected experimentally. These plates and their locations in the inlet section are shown in figures 5 and 6.

Since the final pressure of the compressor chamber depends on the mass flow into pump tube, the compressor chamber volume must be selected to take account of this flow. The gas which flows into the pump tube at a temperature $T_3$ occupies a volume that can be calculated. From equation (A12) this volume is, for a pump tube of diameter $D_{pt}$ and length $l$,

$$V_3 = X_{cs} \frac{\pi}{4} D_{pt}^2 = \frac{X_{cs}}{l} \frac{\pi}{4} l D_{pt}^2 \tag{B10}$$

Thus, with $p_3$ and $T_3$, the mass of the helium which moves from the compressor chamber is known. If adiabatic expansion of the gas in the compressor chamber is assumed for this mass removal, then the required volume of the compressor chamber can be computed with

$$V_4 = V_3 \left(\frac{p_5}{p_4}\right) \left(\frac{T_4}{T_6}\right) \left[1 - \left(\frac{p_5}{p_4}\right)^{\frac{1}{\gamma_4}}\right]^{-1} \tag{B11}$$

where $T_6$ is the temperature of the compressor gas in the pump tube after it has been compressed by the reflected shock. This temperature, with $p_6 = p_5$ and $u_6 = 0$, is

$$\frac{T_6}{T_3} = \frac{\frac{p_5}{p_3}\left(\alpha_4 + \frac{p_5}{p_3}\right)}{1 + \alpha_4 \frac{p_5}{p_3}} \tag{B12}$$

Since it was found that the best match for the pressure ratio $p_4/p_5$ would occur with an effective inlet area ratio only slightly greater than 1, the initial conditions required for total equilibrium were calculated, following the method described in appendix A, for an inlet area ratio of 1.

## REFERENCES


1. Eggers, A. J., Jr., Hansen, C. Frederick, and Cunningham, Bernard E.: Theoretical and Experimental Investigation of the Effect of Yaw on Heat Transfer to Circular Cylinders in Hypersonic Flow. NACA RM A55E02, 1955.

2. Reshotko, Eli, and Beckwith, Ivan E.: Compressible Laminar Boundary Layer Over a Yawed Infinite Cylinder With Heat Transfer and Arbitrary Prandtl Number. NACA TN 3986, 1957.

3. Goodwin, Glen, Creager, Marcus O., and Winkler, Ernest L.: Investigation of Local Heat-Transfer and Pressure Drag Characteristics of a Yawed Circular Cylinder at Supersonic Speeds. NACA RM A55H31, 1956.

4. Stalder, Jackson R., Goodwin, Glen, and Creager, Marcus O.: Heat Transfer to Bodies in a High-Speed Rarefield-Gas Stream. NACA Rep. 1093, 1952. (Supersedes NACA TN 2438)

5. Kovasznay, Leslie S. G., and Tormarck, Sven I. A.: Heat Loss of Hot Wires in Supersonic Flow. Bumblebee Rep. No. 127, Johns Hopkins Univ., Dept. of Aero., Apr. 1950.

6. Stine, Howard A.: Investigation of Heat Transfer From Hot Wires in the Transonic Speed Range. Heat Trans. and Fluid Mech. Inst., Berkeley, Calif., June 30 - July 2, 1954.

7. Feller, William V.: Investigation of Equilibrium Temperatures and Average Laminar Heat-Transfer Coefficients for the Front Half of Swept Circular Cylinders at a Mach Number of 6.9. NACA RM L55F08a, 1955.

8. Logan, Joseph G., Jr.: Relaxation Phenomena in Hypersonic Aerodynamics. IAS Preprint No. 728, 1957.

9. Hansen, C. Frederick: Approximations for the Thermodynamic and Transport Properties of High-Temperature Air. NACA TN 4150, 1958.

10. Glass, I. I., and Patterson, G. N.: A Theoretical and Experimental Study of Shock-Tube Flows. Jour. Aero. Sci., vol. 22, no. 2, 1955, pp. 73-100.

11. Hertzberg, A., Smith, W. E., Glick, H. S., and Squire, W.: Modifications of the Shock Tube for the Generation of Hypersonic Flow. Rep. AD-789-A-2, Cornell Aero. Lab., Inc., March 1955.

12. Dosanjh, Darshan Singh: Use of a Hot-Wire Anemometer in Shock Tube Investigations. NACA TN 3163, 1954.

13. Hertzberg, A.: The Shock Tunnel and Its Applications to Hypersonic Flight. Rep. No. AD-1052-A-5, Cornell Aero. Lab., Inc., June 1957.

14. Glass, I. I., Martin, W., and Patterson, G. N.: A Theoretical and Experimental Study of the Shock Tube. UTIA Rep. No. 2, Univ. of Toronto, Inst. of Aerophysics, Nov. 1953.

15. Dosanjh, Darshan Singh: Interaction of Grids With Traveling Shock Waves. NACA TN 3680, 1956.

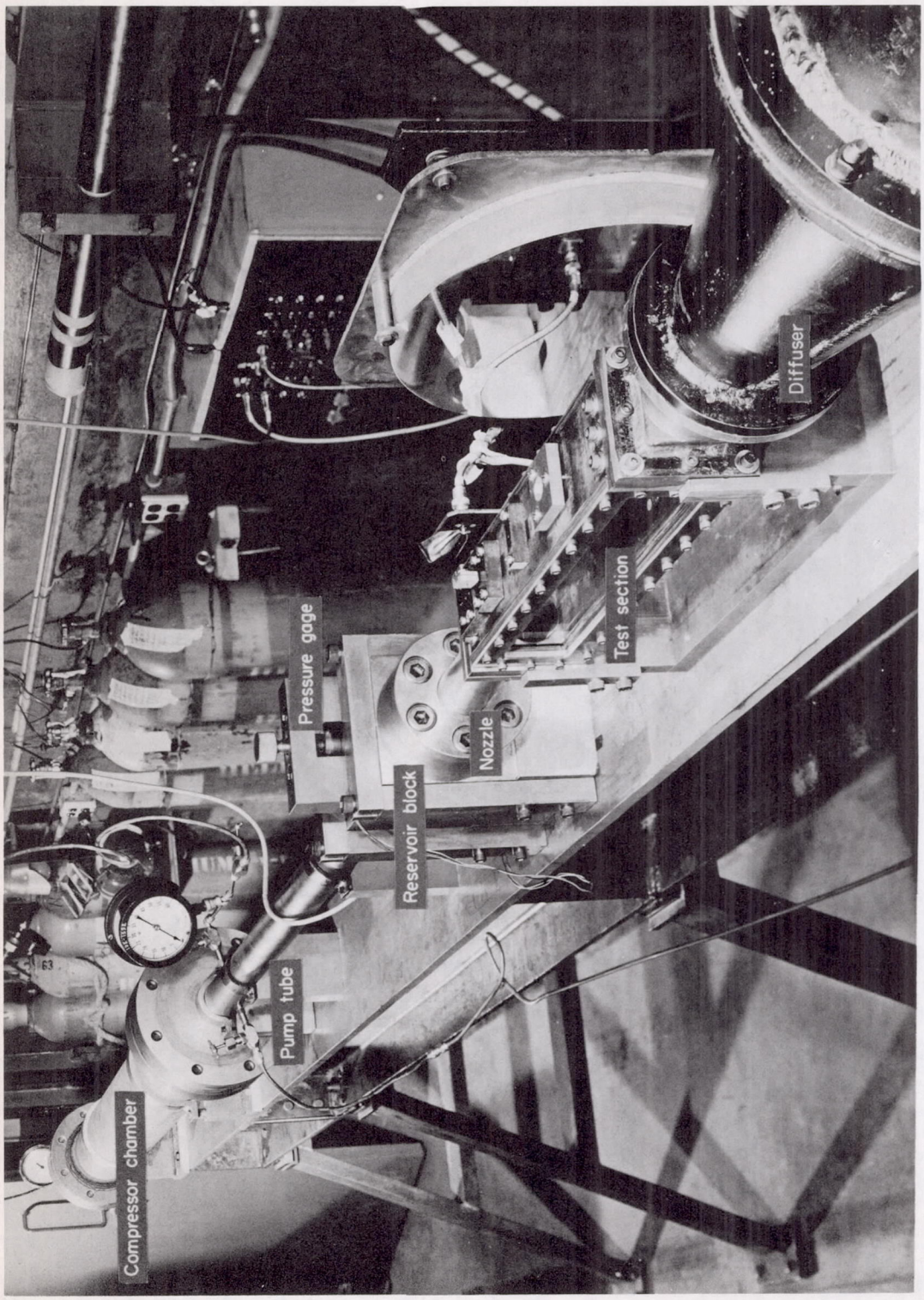



Figure 1.- The test apparatus.

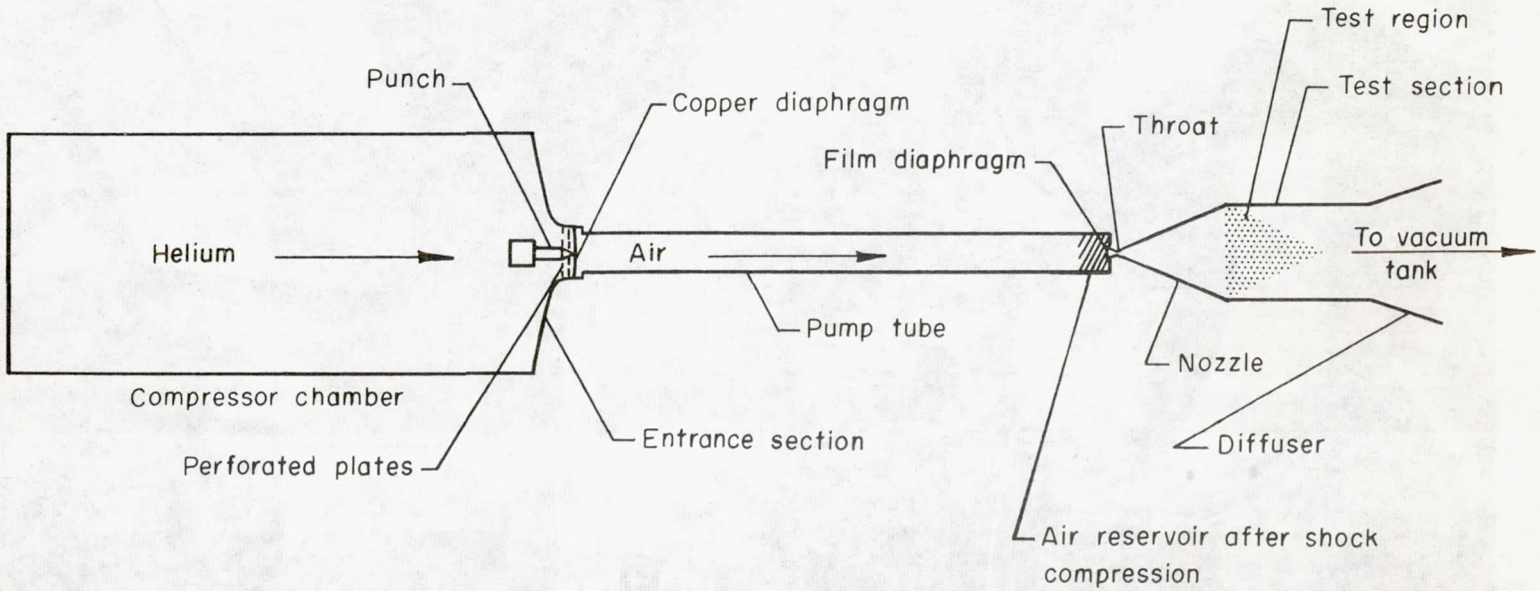
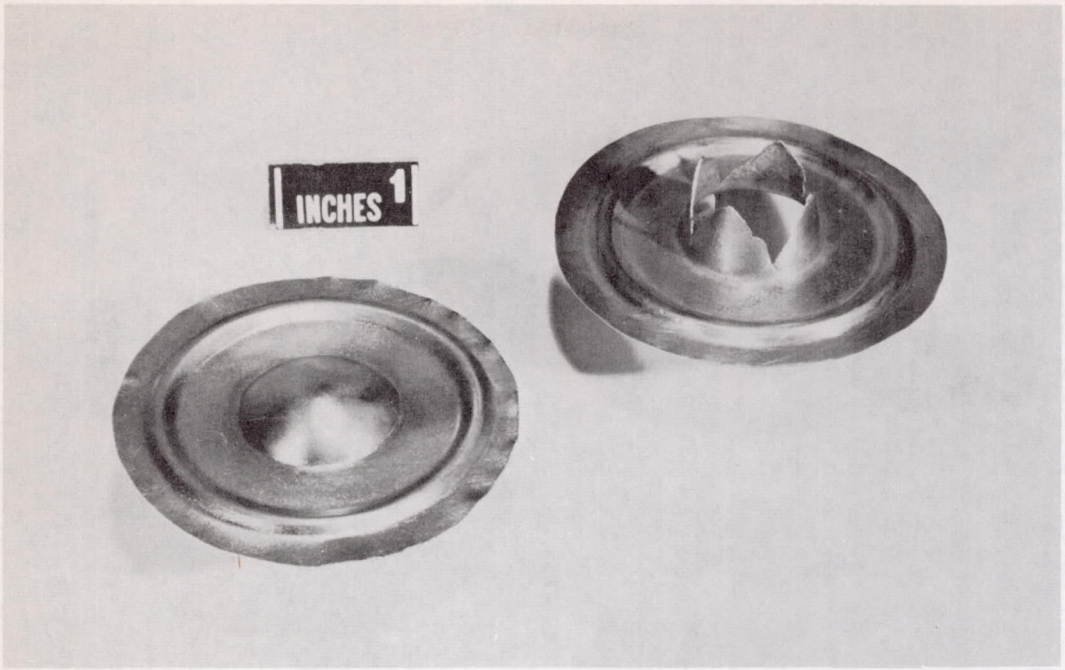
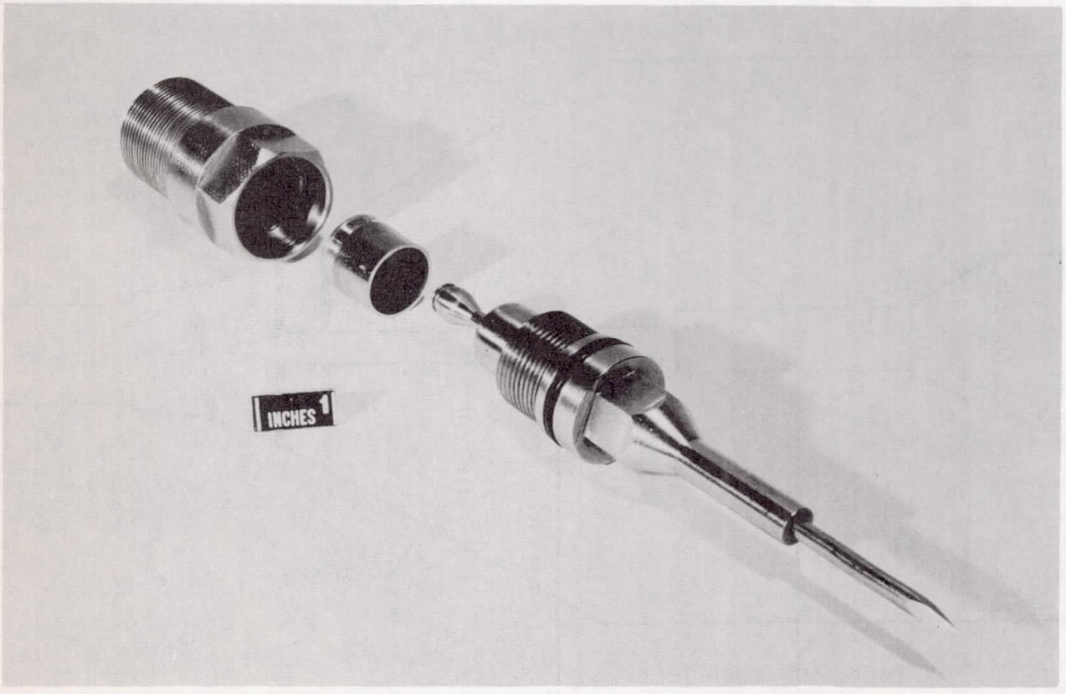



Figure 2.- Schematic diagram of the test apparatus.



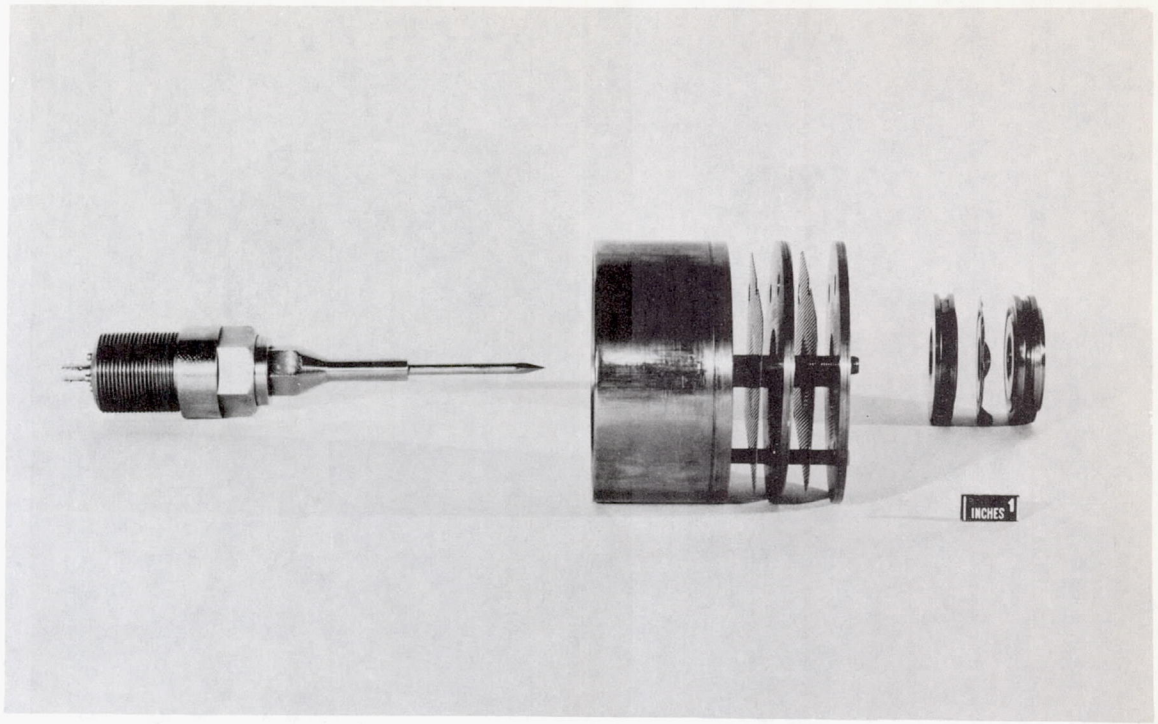

A-22851

Figure 3.- Shaped copper diaphragm before installation and a diaphragm after rupture.




A-22848

Figure 4.- Component parts of punch with which diaphragm is pierced to start rupture.




A-22847

Figure 5.- Punch and inlet assembly shown in the order of installation.

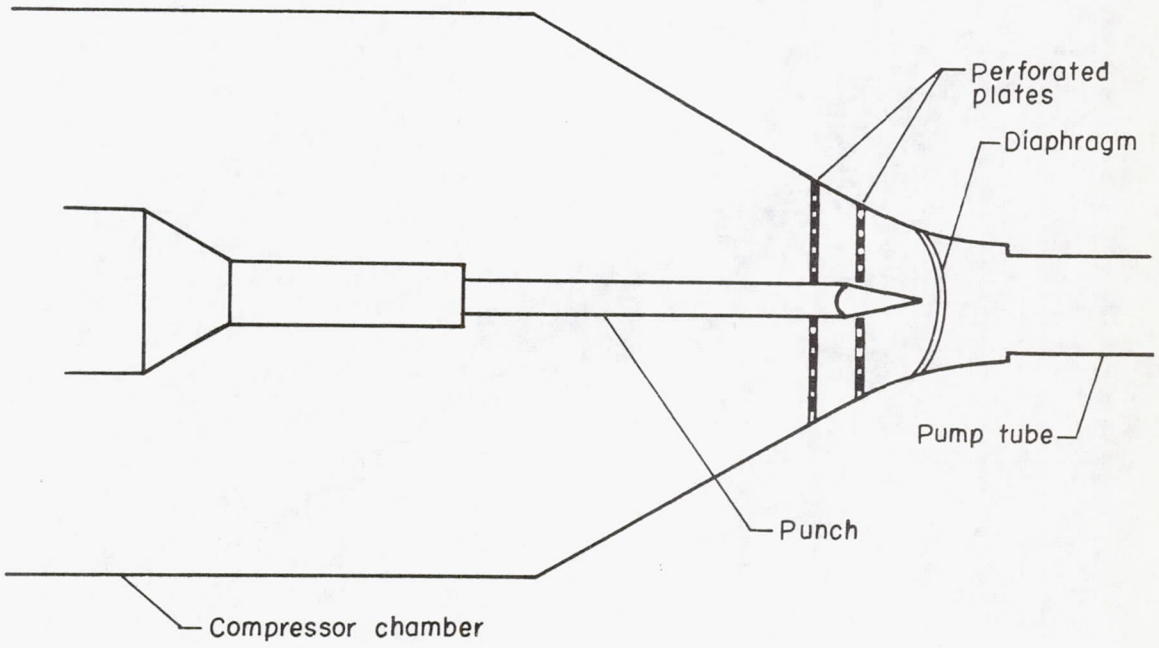
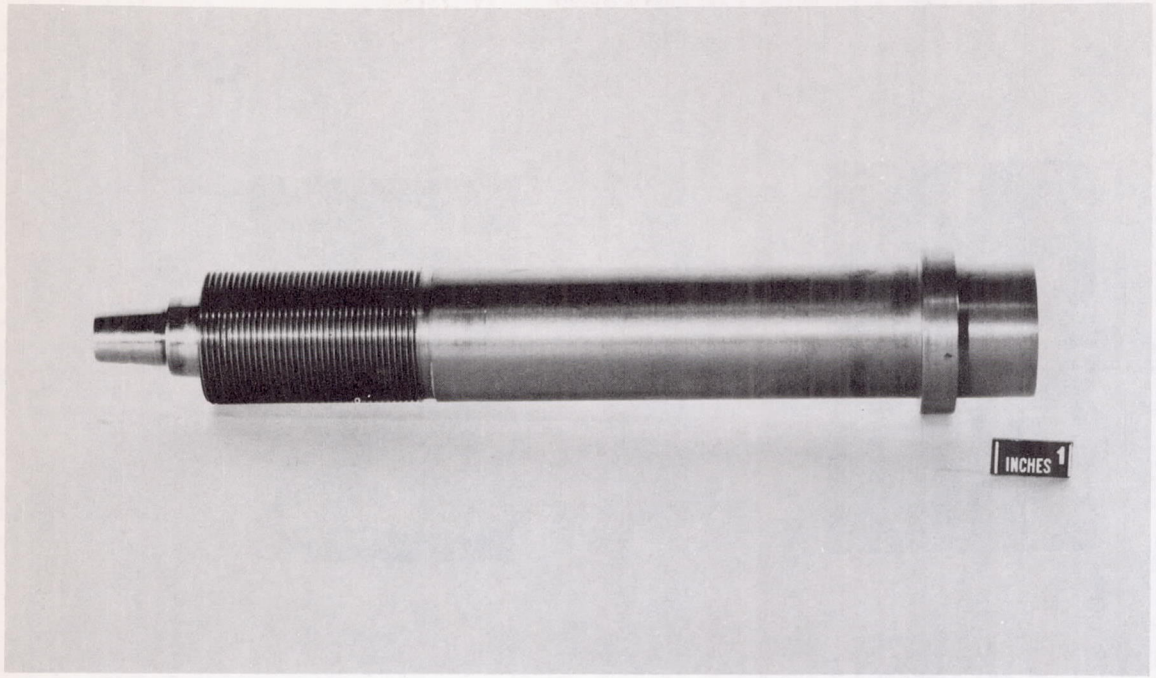
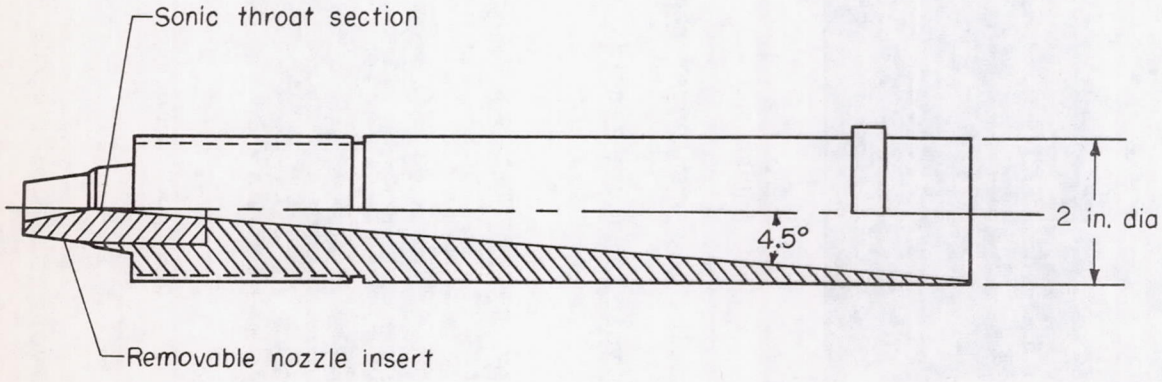



Figure 6.- Schematic diagram of inlet section showing perforated plates with which flow is throttled.

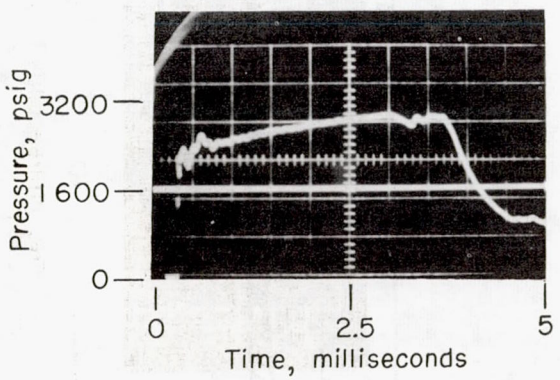



(a) Photograph of nozzle.

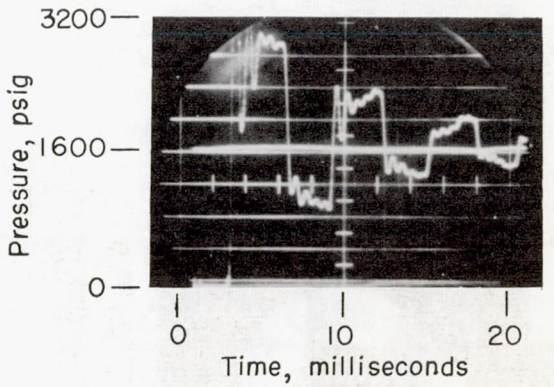



(b) Schematic diagram of nozzle.

Figure 7.- Nozzle for the test apparatus.

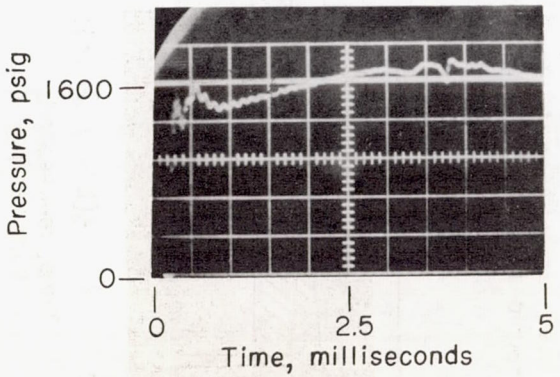



(a) Piezoelectric transducer record.

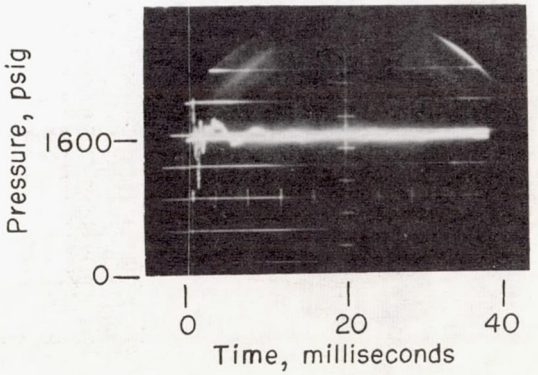



(b) Strain-gage record.

Figure 8.- Reservoir pressure records showing pressure fluctuations when throttling plates were not used.




(a) Piezoelectric transducer record.




(b) Strain-gage record.

Figure 9.- Reservoir pressure records showing pressure fluctuations when effective throttling was established.

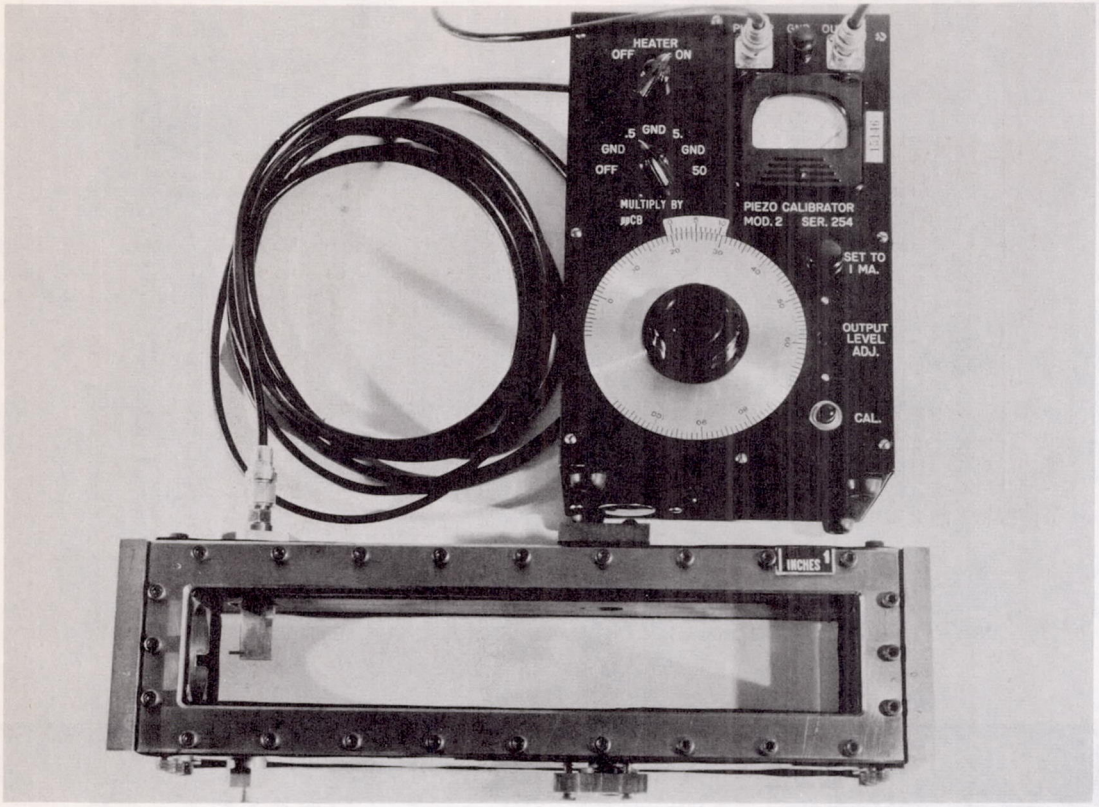
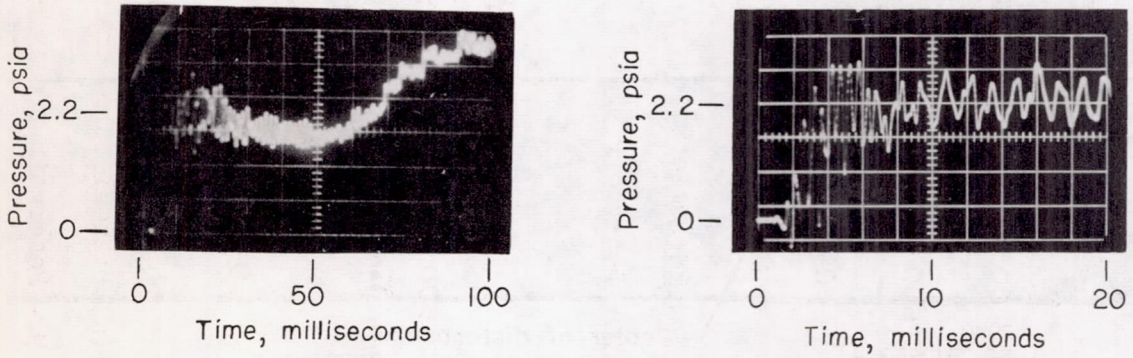



Figure 10.- Pitot-pressure probe and piezoelectric pressure transducer installed in test section with calibrator-attenuator attached.




(a) Duration of hypersonic flow. (b) First 20 milliseconds of flow.

Figure 11.- Pitot-pressure records.

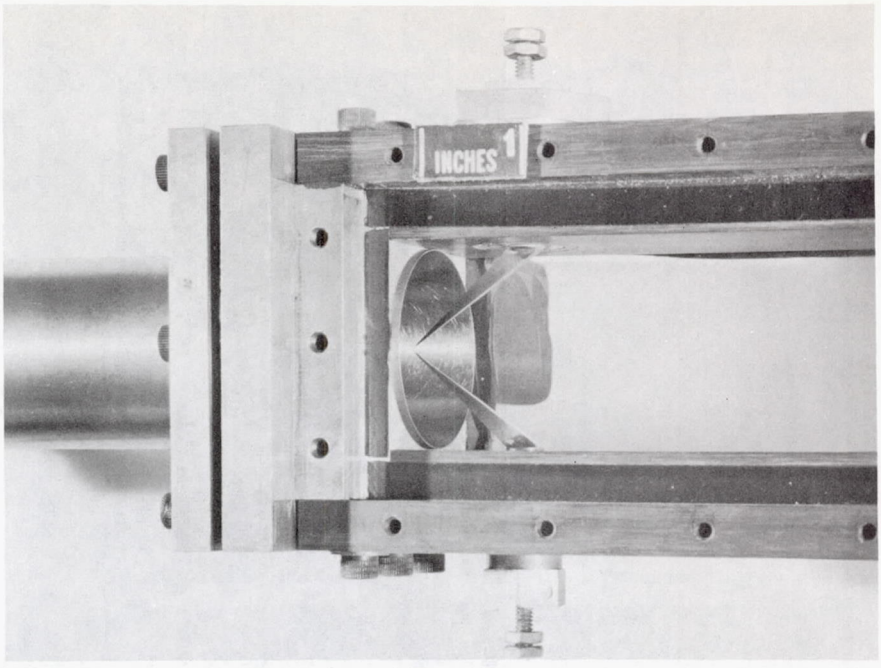
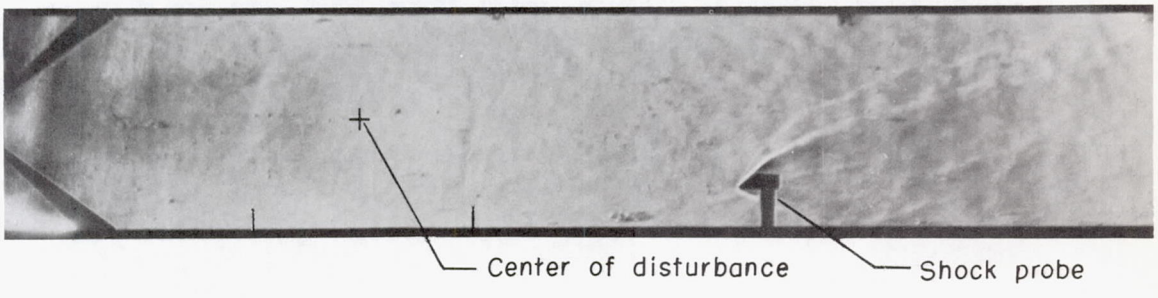
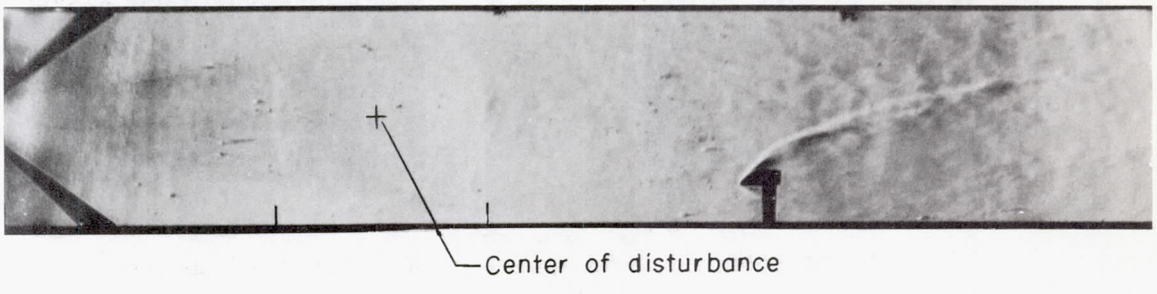



Figure 12.- Disturbance spark electrodes mounted in test section.




(a) 2 milliseconds after start of flow; delay time = 46 microseconds.




(b) 27 milliseconds after start of flow; delay time = 47 microseconds.

Figure 13.- Schlieren photographs of the spark discharge sweeping through the test section.

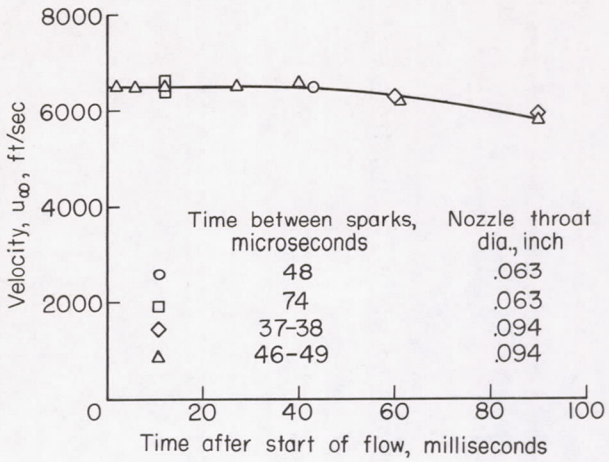
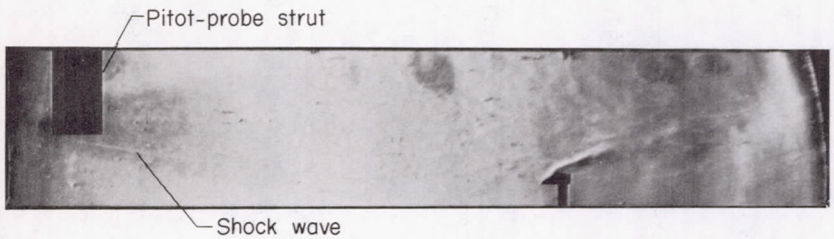
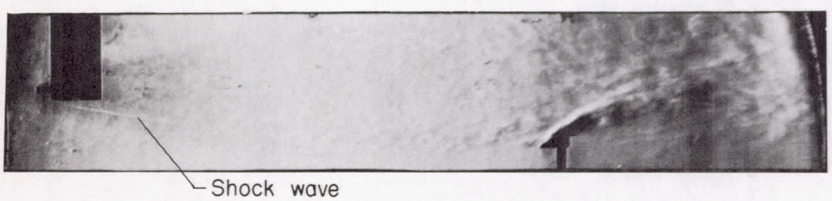



Figure 14.- Free-stream velocity as a function of time.




(a) 0.063-inch-diameter sonic throat; M = 10.4.




(b) 0.094-inch-diameter sonic throat; M = 9.5.

Figure 15.- Mach number determined from the angle of the shock wave from pitot-probe strut.

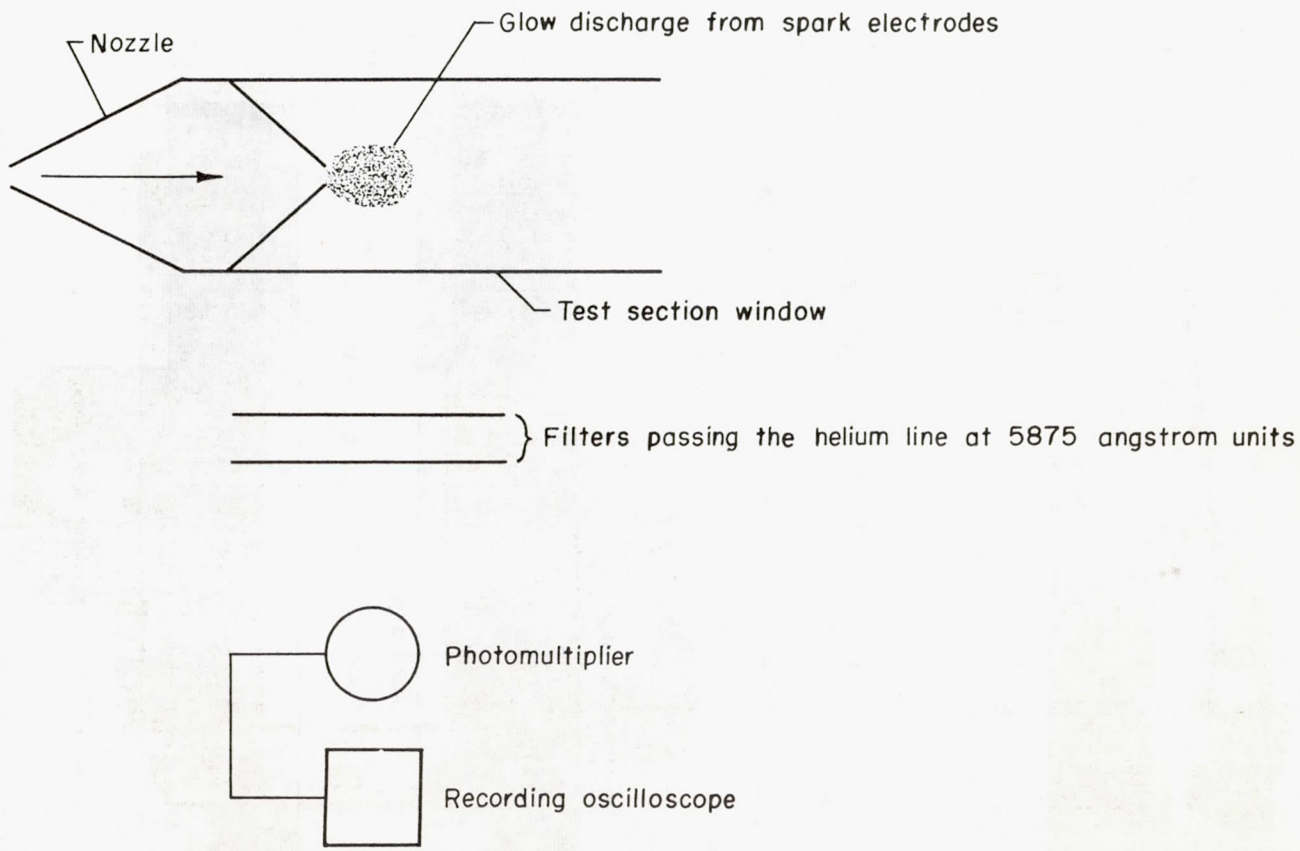
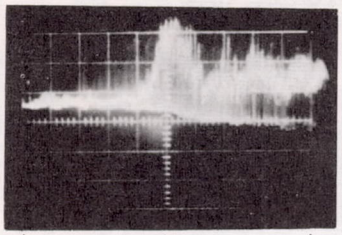



Figure 16.- Schematic diagram of helium detector.




Helium first detected
40 milliseconds after
start of flow

Figure 17.- Typical record of the output from the helium detector.

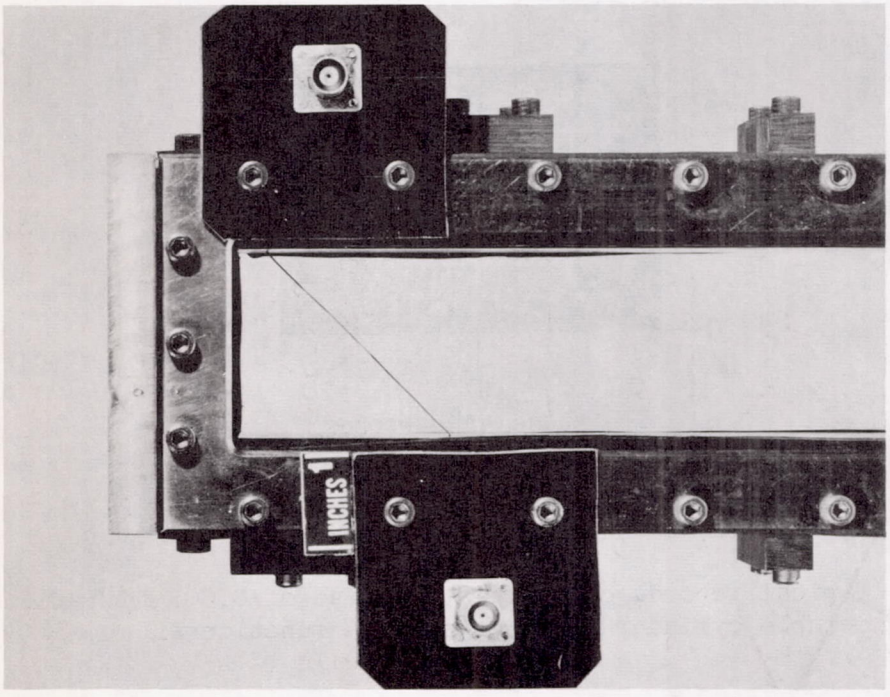
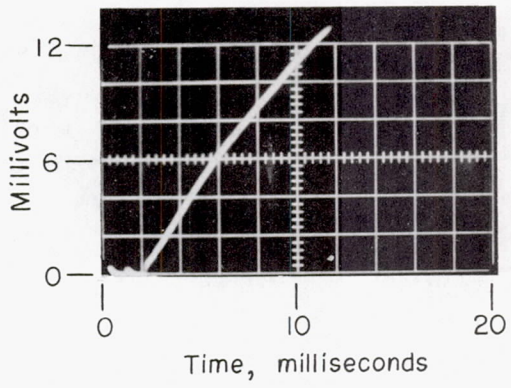
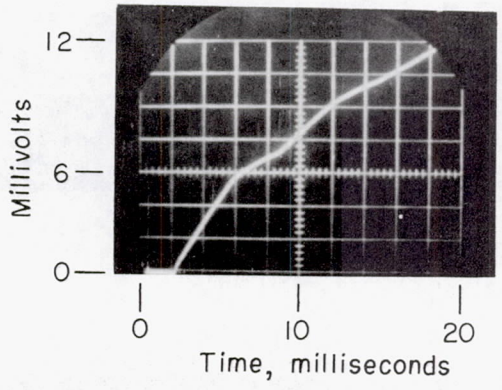



Figure 18.- Photograph of typical installation of heat-transfer model; a 0.020-inch-diameter thermocouple cylinder mounted in the test section at 45° angle of yaw.

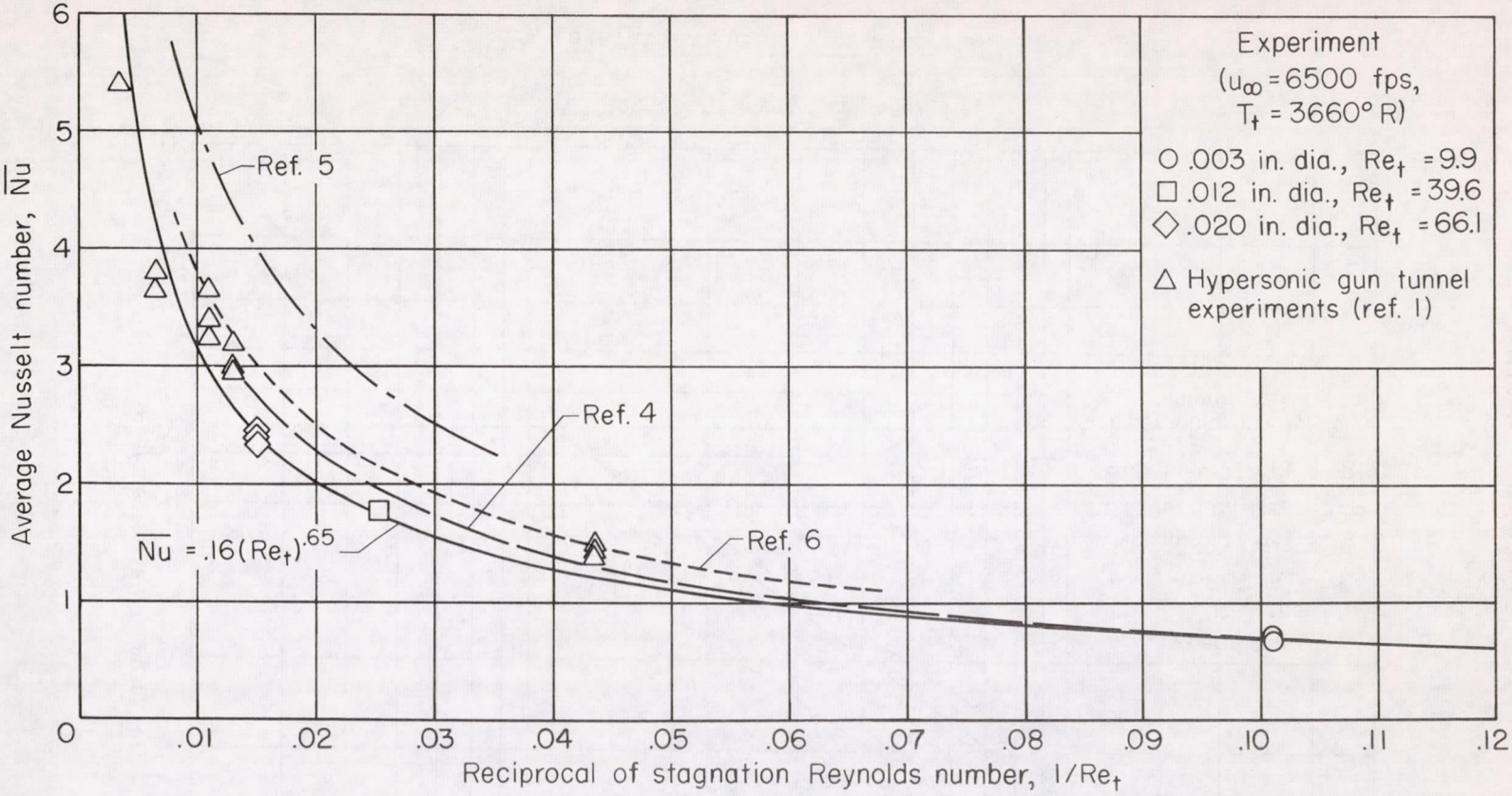



(a) Test in which throttling plates were used.



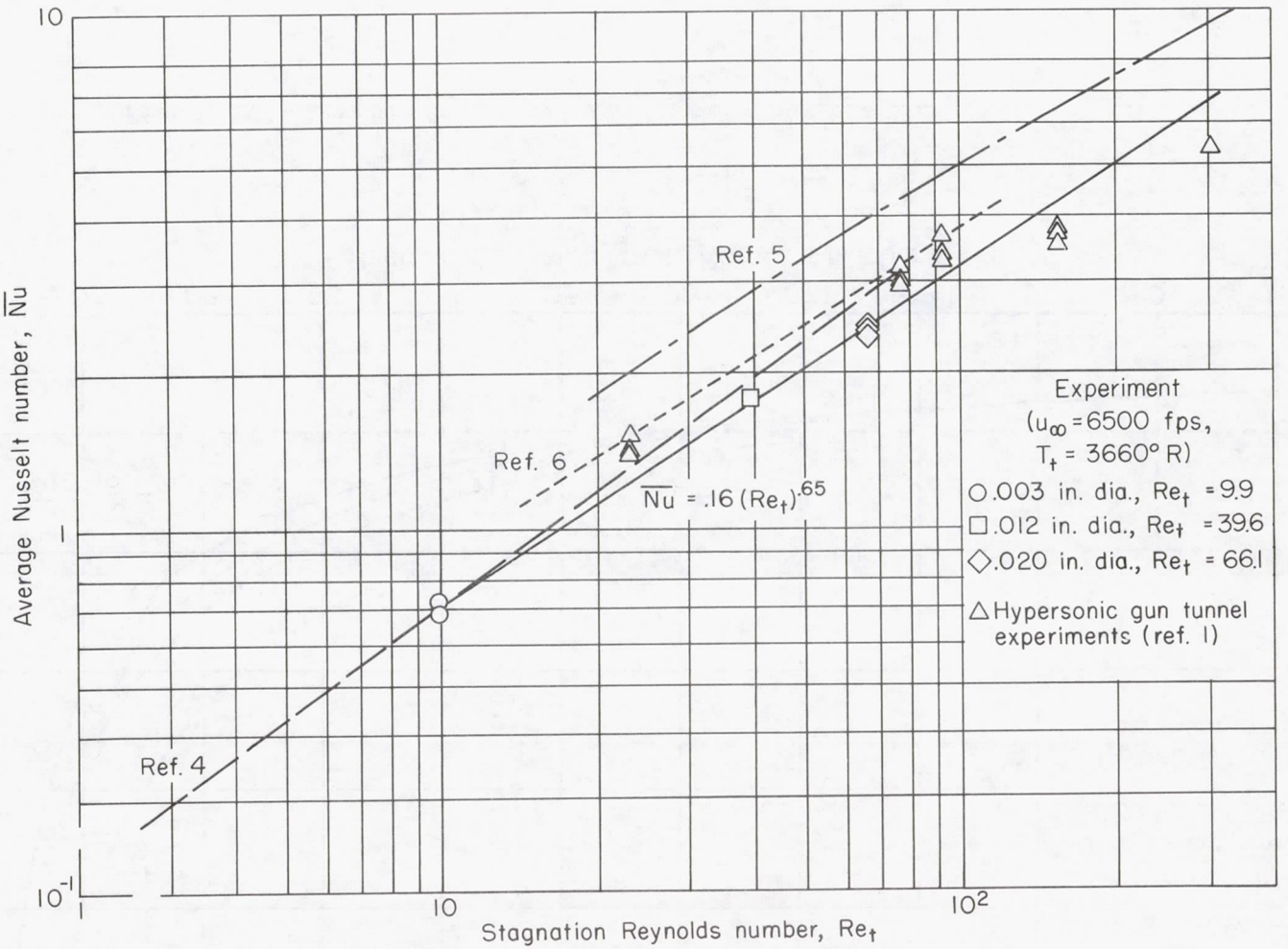

(b) Test in which no throttling plates were used.

Figure 19.- Typical records of temperature rise of 0.003-inch-diameter thermocouple cylinder at zero yaw as a function of time.




(a) Variation of $\overline{Nu}$ with $1/Re_t$.

Figure 20.- Comparison of average Nusselt numbers for cylinders transverse to flow.




(b) Variation of $\overline{Nu}$ with $Re_t$.

Figure 20.- Concluded.

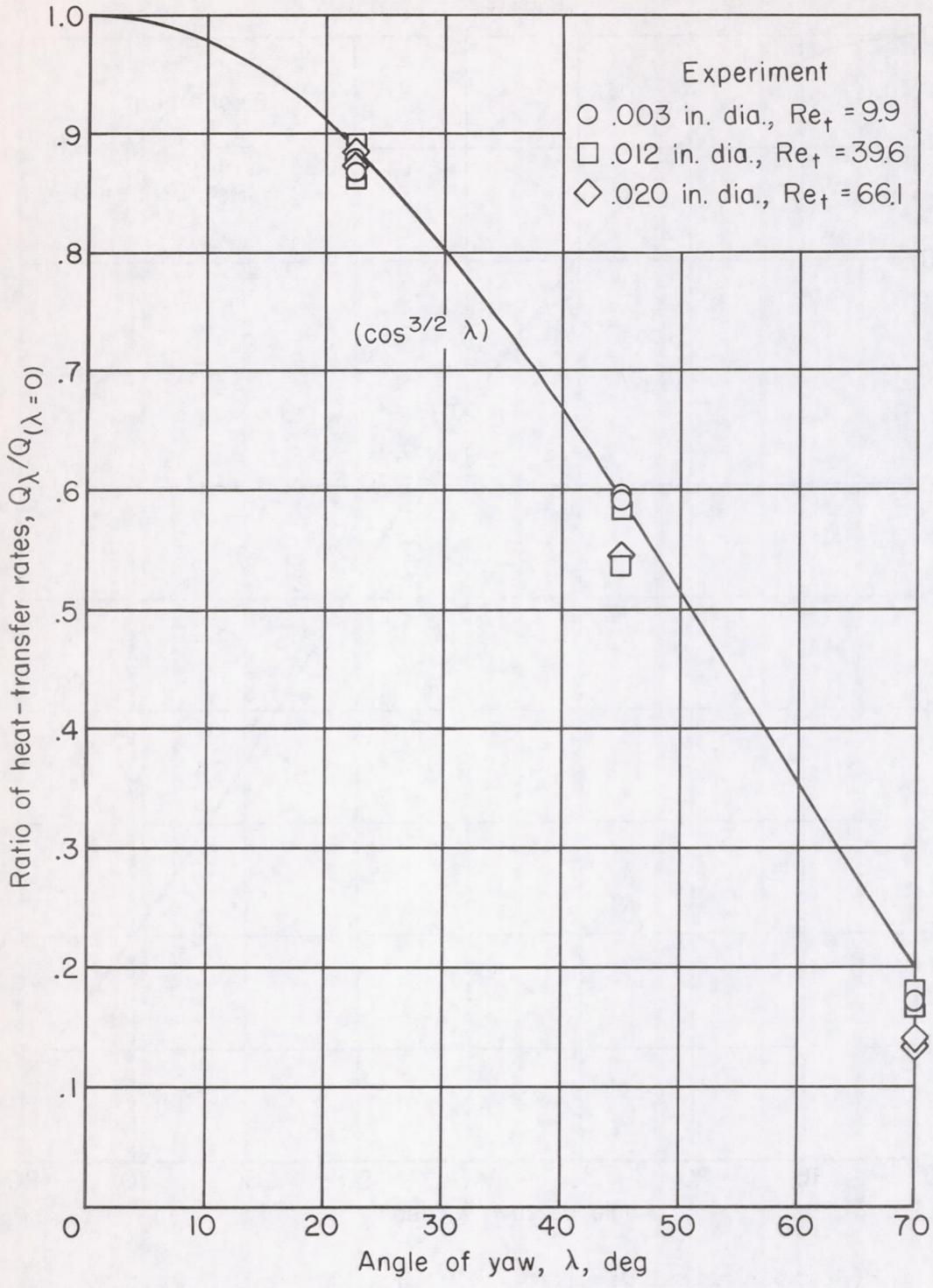



Figure 21.- Comparison of theory and experiment of the influence of yaw on the rate of heat transfer to cylinders in high-velocity flow; M = 11, $T_t$ = 3660° R, $Re_t$ = 4.0×10⁴ per foot.

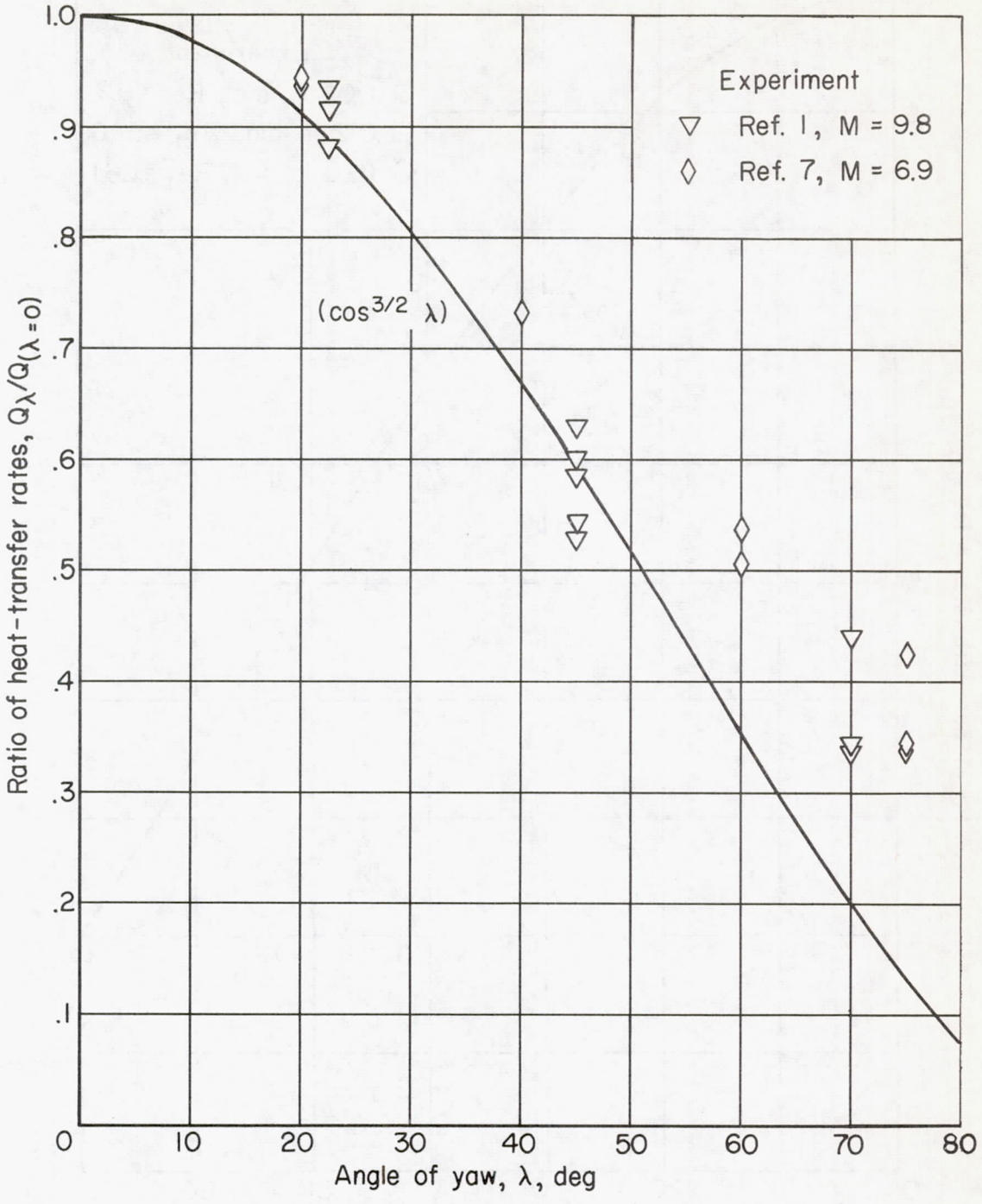



Figure 22.- Experimental data from references 1 and 7 showing the influence of yaw on average rates of heat transfer to cylinders in high Mach number flow.

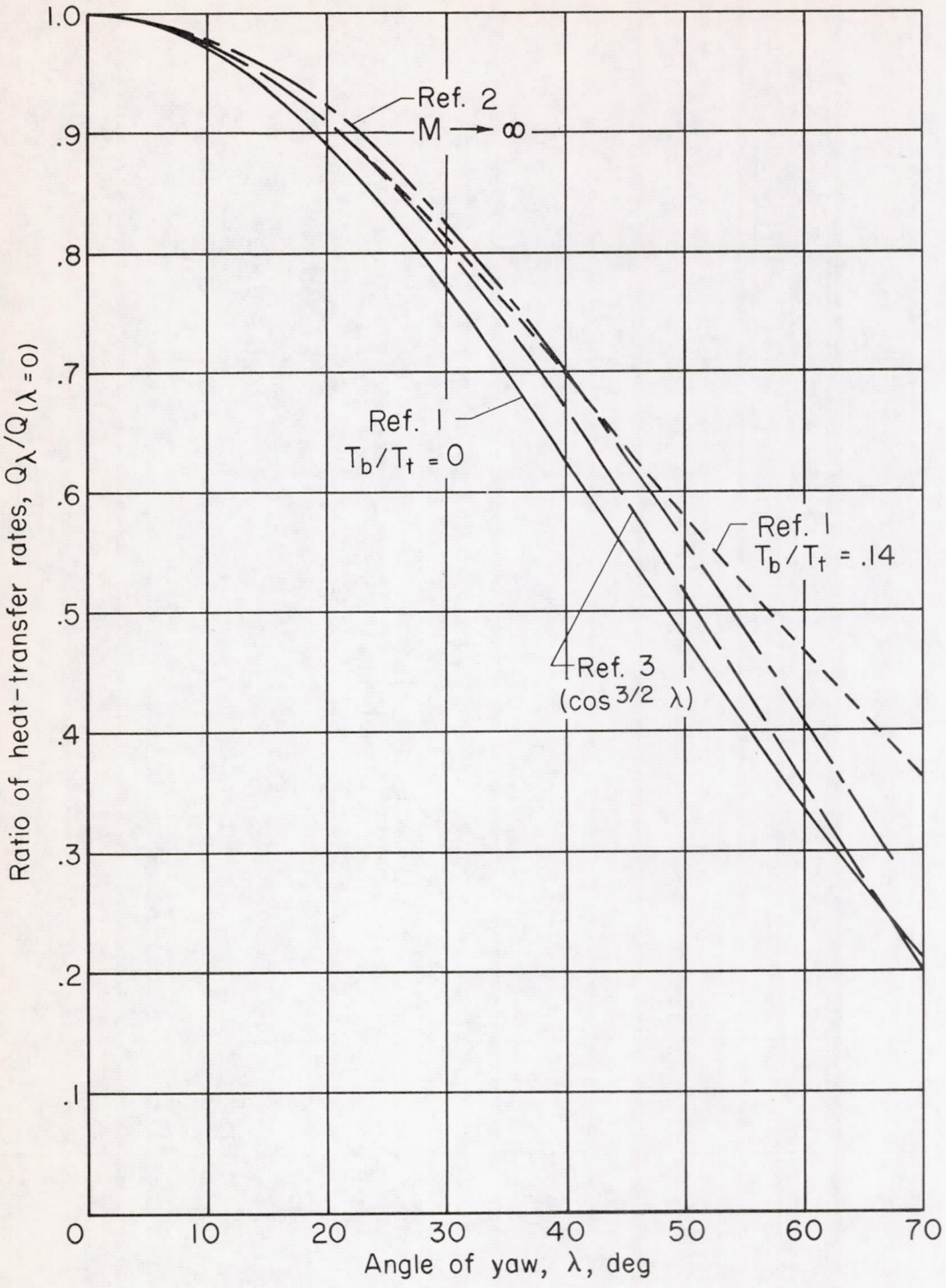



Figure 23.- Influence of yaw on heat-transfer rates to a cylindrical stagnation region in high Mach number flow as predicted by various theories.